Review | Received 15 September 2023; Accepted 26 November 2023; Published 4 December 2023
https://doi.org/10.55092/am20230003

Review of surface measurement methods towards non-destructive internal surface assessment

Kwan Zhi Teh[1,2], Saikat Medya[1,2], Sugandhana Shanmuganathan[1,2], Swee Hock Yeo[1,2,*]

[1] School of Mechanical and Aerospace Engineering, Nanyang Technological University, Singapore
[2] Rolls-Royce@NTU Corporate Laboratory, Nanyang Technological University, Singapore

* Correspondence author; E-mail: mshyeo@ntu.edu.sg.

Abstract: Metal additive manufacturing techniques have enabled the ability to construct complex internal channels, but they create rough surfaces of varying qualities. Surface texture is vital to engineering analysis and is usually emblematic of product quality. The problem, however, lies with the difficulty in measuring or assessing such internal surfaces. As they are concealed by nature, it is difficult to measure them non-destructively through conventional measurement methods. Non-destructive means are favored as they save materials and time, but a proper review of less-known available methods is first required to reveal and understand the proper means of evaluating internal surface non-destructively. This paper reviews the measurement methods of capacitance, vibration analysis, optical techniques, X-ray computed tomography, and replica methods critically with their working principles, pros and cons discussed. Their current applications in literature are evaluated to understand the appropriateness for internal surface applications. Endoscopic non-destructive testing (NDT), X-ray computed tomography, and replica methods are found to be rather suitable. Propositions are also given for enabling the less suitable methods. Amongst all these techniques, X-ray computed tomography stands out as a great method for such purposes and would appear to be the best path forward for development, provided that its resolution issues are improved through better reconstruction algorithms, novel scanning methodologies, or improved X-ray energy sources.

Keywords: Surface; measurement techniques; review and evaluation; non-destructive; internal; replica; X-ray CT; optical technique; vibration; capacitance

1. Introduction

The rise in metal additive manufacturing techniques such as directed energy deposition (DED), binder jetting, sheet lamination, powder bed fusion (PBF) and its variations have led to the ability to construct complex components that were previously unfeasible, for example, intricate internal channels. Through additive manufacturing, material wastage can be reduced in contrast to conventional methods of subtractive manufacturing. Its drawback of creating

rough surfaces, print defects [1], has however, dissuaded certain practical product applications due to the surface quality. Surface condition is vital to engineering analysis, and generally emblematic of product quality. Within internal channel context, rough, defective surfaces result in larger frictional energy losses [2], boundary layer disruptions, higher flow turbulence, and worse fatigue properties due to the existence of more stress concentration sites [3]. Flow perturbations are most generally considered undesirable within channels, and the issue of fatigue shows its importance when the channel is part of a system that vibrates in operation, for example, the cooling and transport channels in engines. The merits of having such surface information are evident, but the assessment of such concealed textures has proven to be a conundrum due to their inaccessibility. Unlike external surfaces that can be easily examined through styluses, microscopes, and other conventional methods, internal surfaces require either destruction for assessment, or a non-destructive means of measurement. Destructive means, though simple to integrate with conventional instruments, will result in extra material, time, and monetary costs, due to the extra step of component slicing. Non-destructive testing techniques for surface measurements have been used for more than 30 years. It involves assessing and analyzing the properties of a system, component or an individual material without altering them [4]. These techniques are applied in diversified fields as they can detect faults without hindering the operation process of any equipment. Hence, another term: non-destructive evaluation (NDE) is also used to describe this technology [5,6]. They can create the preface to estimating mechanical parameters for materials exploited for a long temporal period, even after influences by welding procedures [7]. Commonly used NDT methods at present include ultrasonic wave testing, eddy current testing, microwave and acoustic emission, electromagnetic testing, radiography testing, liquid penetration testing, visual inspection, and magnetic particle testing. These common NDT methods are catered towards varying parameters that are not very inclusive of surface evaluation. It is clear, however, that forms of non-destructive surface measurement would alleviate the costs, and would be very much desirable in an industrial setting. The internal surfaces could be inspected in-situ, without harm, and hence lead to direct quality assurance. Contrast this to destructive methods, where sacrificial samples are needed for repeated measurements, with the quality assurance drawn from historical data, and the assumption that the sample represents the population sufficiently.

Presently, there is a literature gap in that no assessment of the surface measurement scene has been done within the context of internal/concealed surfaces. This paper is hence penned to review current available technologies and concepts of measuring, inspecting surfaces, to reveal the most suitable paths forward for developing an efficient and viable internal surface measurement method, and serves as a primer, reference to other upcoming work in surface measurement technologies. The paper also consolidates multiple measurement techniques of different principles within one review for a cross-domain perspective on surface measurement, which would be highly informative for the appropriate selection of technology for practical application.

2. Development of surface measurement

Early days of roughness "measurement" were done through touch or sight by the human senses, and technologies have attempted to reenact these senses in multiple forms. The foremost challenge at the time was quantifying surface qualities: to turn the senses into measurable numbers. Abbott and Firestone's elementary work on this topic in 1933 [8] (see Figure 1) first paved the path for the development of surface texture characterization. A curve was put forward to represent the surface in terms of height distribution against material ratio: at every height datum the material fraction percentage is given, and hence a mean line is obtainable. This work then led to the formation of various roughness, filter parameters and analysis techniques [9].

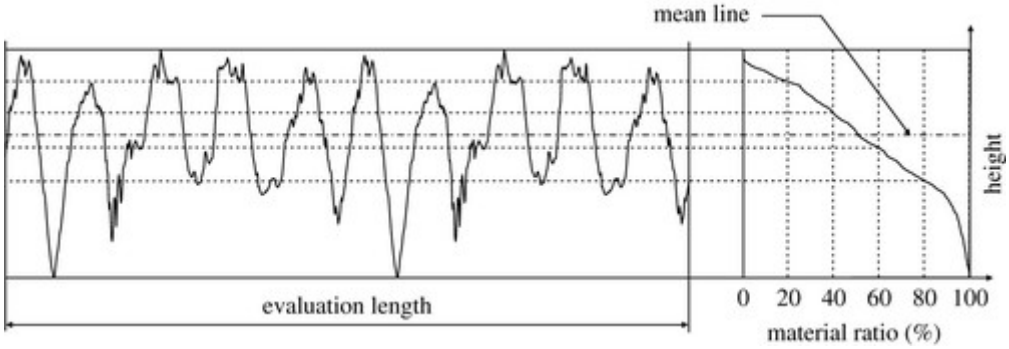

Figure 1. The Abbott-Firestone curve [9], reproduced with permission. Copyright© 2007 The Royal Society.

Subsequent instrument developments resulted in the introduction of the first stylus instrument "Talysurf" in 1941 by Taylor Hobson [9,10]. The "sight" form of measurement had also seen attempts of reprisal in the form of optical methods. The first trial could be traced back to Schmalz in 1929, who tried to magnify normal surface view with an angled strip of light [9]. Davies then presented a probability-based model of rough surface reflections [11], and kickstarted the use of specular reflectance principles for surface measurement with Gaussian surface height distribution assumptions, as seen in experimental validation by Birkebak's dissertation [12]. Thereafter, Sprague introduced a novel promising method based on speckle patterns interferometry in 1972, which showed good correlation with stylus measurements over diversely finished surfaces [13].

The origin of non-contact instruments could be traced back to a diffraction-based optical profiler that was described in a 1975 paper [14], followed by the several non-destructive instruments to come. The miniaturization in scale is evident with the introduction of Scanning Tunneling Microscopy (STM) in 1983 [15], an application of the vacuum tunneling phenomenon. Subsequently, the Atomic Force Microscopy (AFM) that built upon STM and utilizes repulsive van der Waal's force was introduced in 1986 [16]. Both methods are capable of atomic-scale imaging for nanoscale surface quality analysis. Such a scale shift could be attributed to accommodating the upcoming rise in nanotechnology and precision engineering in early 2000s, hence the need for characterizing surface conditions of miniature

products [17]. The advent and subsequent advancement of the digital age increases available computing power, and pushes surface measurement techniques towards the trend of data analytics. Machine learning, image recognition, and other sophisticated models are employed to analyze signals and provide relevant surface information. As measurement technologies are largely mature at this stage, the field becomes more of a competition of signal analysis over signal acquisition. Presently, there is a trend to advance towards Industry 4.0 enablers, utilizing digitalization, internet connectivity and sensor fusion to achieve either more efficient, or more accurate measurements. Despite these, measurement principles still form the basis of surface characterization, and it is hence necessary to have an overview of the fundamentals.

3. Existing surface measurement methods

There exists a multitude of surface measurement techniques that are either heavily commercialized or has seen extensive usage in laboratory environments. Figure 2 shows a classification of such techniques. Surface measurement techniques can be classified under two large sections–one of profilometry, where direct surface information is extractable; and the other of representative methods, where a proxy value or indicator is used to represent the surface condition. It is obvious that not all the current techniques are applicable to measuring internal surfaces non-destructively. As part of the review, the principles and development of the less-known techniques available are examined to illustrate their suitability or shortcomings in this aspect. Common techniques such as stylus and the vast majority of electron, tunneling, white-light microscopy will not be examined in this as their purposes and working mechanisms are rather well-known.

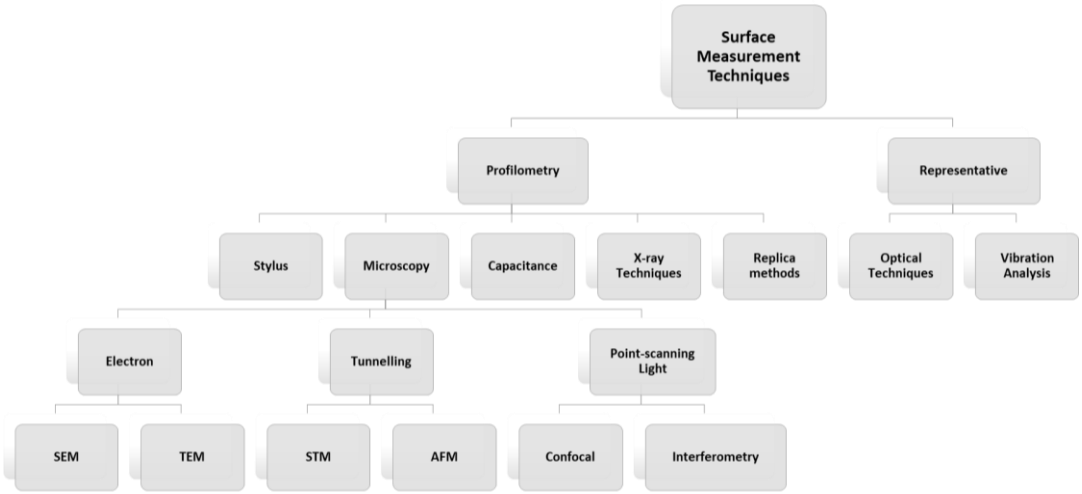

Figure 2. A broad categorization of existing surface measurement techniques.

4. Capacitance

Capacitance based surface measurement is a non-optical, electrical technique that utilizes a capacitive displacement sensor also known as a capacitive proximity sensor which operates by change in electrical capacitance. Two plates separated by an insulator material or medium,

out of which, one plate is within the sensor that is connected to the oscillator circuit that generates the electrostatic field, and the target acts as the other plate. As the distance between the two plates increases, the oscillation amplitude decreases, which changes the capacitance in the field. The sensor's component groups are most commonly arranged in the cylindrical format (refer to [18]). While using this sensor for surface measurements, this means the sensor plate is unequal in length compared to target surface, in which case the fringing effect at the edges can affect the resolution of measurement. This can be counteracted by having a smaller distance between the plates (probe to target). To analyze surface finish of samples, the sensor scans across the surface and the distance changes caused by swarf, burrs and defects are collected by the controller that processes the data. The sensor is non-contact type when the dielectric insulator medium is air, which is the one used for surface profilometry and makes it suitable for in-process measurements and monitoring.

The first attempt to measure surface profile in-process on a turned surface was done by Garbini *et al.* [19] using a Fringe Field Capacitance (FFC) sensor. There was variation observed in the fringe field due to the change in displacement owing to the surface roughness. Subsequent works in the field emphasized on influence of different parameters (Range, Standoff, Output Voltage, Linearity Error, Resolution, Sensing diameter, *etc.*,) of the instrument on the measurement, different shaping processes, and comparison with stylus profilometry measurements [19]–all of which is briefed in [18] of Murugarajan *et al.* who proposed and experimented a capacitance-sensor-based-surface roughness system on ground, milled and shaped surfaces. They generated their surface profiles and reported that the sensor performed better on ground surfaces (moderately rough) than milled or shaped (very rough surfaces) ones and that to generate a profile, the sensor diameter should be less than the peak-to-peak distance. The following capacitance response model was used to calculate Capacitance Roughness R_c from measured Capacitance C.

The capacitive sensor used to measure the surface roughness consists of a sensing element which acts as one of the conducting capacitor plates [18], while the machined surface (target) forms the other conducting plate. If the sensing area and dielectric conductivity are both held constant, the capacitance (C) will be inversely proportional to the average distance (Z_m) between the two conductive plates. The capacitance is given by,

$$C = K \iint_A \frac{dxdy}{Z} \; or \; \frac{KA}{Z_m} \tag{1}$$

where: K is the dielectric constant and Z_m is reciprocal of the mean value of $1/Z$ over area A. If the surface finish is represented by the function $z = f(x,y)$ then the distance between the plates is given by $Z = a_d + f(x,y)$, where a_d is the standoff distance normally fixed for a given sensor by means of zero setting arrangement of the driver electronics.

$$\frac{1}{Z_m} = \frac{1}{A} \iint_A \frac{dxdy}{a_d + f(x,y)} \tag{2}$$

The observed displacement is an indication of the roughness of the surface on that location spotted (focused) by the sensing element and it is named capacitance surface roughness (*Rc*).

$$R_c = Z_m - a_d \quad (3)$$

The work was further incorporated (sensor and specimen specifications) by Mathiyazhagan *et al.* to study the capacitance response of the surface over three different standoff distances–20 µm, 25 µm, and 50 µm and concluded that 50 µm had the highest correlation factor for all three types of specimens. Although obtaining roughness from a generated profile is established in the above-mentioned works, the pattern of capacitance change for roughness change in single-shot measurement was done in [20,21]. Mathiyazhagan *et al.* in this one, developed a capacitance-sensor-based micro gantry system using a single-shot approach for surface roughness measurement of vertically milled specimens. They investigated selection of an appropriate stand-off distance for the sensing diameter of 5.6mm and concluded that for stand-off distance of up to 500 um, the sensor has higher sensitivity, and after 500 µm, the response to distance change shows a very minimal change. This method can be used for on-line, on-machine [22] measurement in mass production after removing coolant during machining. But Nowichi *et al.* used the FFC method and investigated the influence of coolant during on-line conditions. It has a significant effect on roughness measurement as the presence of coolant alters the dielectric constant of the sensor. A pneumatic cleaning head is suggested to avoid coolant influence on measurement [23]. A review on advanced on-line manufacturing [24] used capacitive sensors to measure the thickness of conductive silver traces on PET substrates that was approximately 4 microns and cross-validated the measurement to be accurate.

Investigation of applying capacitive sensor-based surface measurement for internal surfaces started with the need to measure drilled hole diameters off-line and in-process for aerospace applications. But the wavelengths of diameter variations, as well as surface flaws, are often smaller than the sensing diameter of the probe, hence resulting in low resolution of measurements that fail to identify flaws such as surface gaps and waviness [25]. In [25], Garbini *et al.* experimented with a robot mounted-hole probe that can rapidly and accurately measure both surface profile variations and geometric variations in-process, in the range of 0 to 5 µm and 0 to 1000 µm respectively. Four FFC sensors were radially arranged on the cylindrical tip of the hole probe that measured holes of nominal diameter 6.528 mm with roughness estimates over range of 0.1 to 3 µm. The study concluded that bores with diameters less than 5 mm can be inspected accurately using the instrument. Further, G.Y. Tian *et al.* used a miniaturized capacitive sensing element mounted on a contact-based sensor to measure diameters of deep holes in high resolution. The transducer has two contact probes that transmit the displacement directly onto the non-contact sensing coils. The method was able to measure 3 m long pipes with resolution of 1 µm and an accuracy of 5 µm [26] but there was no surface profile assessment done using this transducer setup.

Capacitance based techniques are predominantly used for surface measurement of external and planar surfaces and their usage is restricted to thin metals, semiconductors, and

polymers [20]. In both profilometry and single-shot approach, Average Surface Roughness (R_a) is the only measure studied. The sensor shows variation in capacitance while detecting surface irregularities, but there is no way to differentiate or quantify. Negative influence of environmental factors like humidity and moisture on the sensing elements are high. Regarding internal surface measurement, not much work is reported other than diameter and surface roughness measurement of straight drilled holes. Work on non-circular channels, channels with varying cross sections, or bent channels are not reported. A flexible endoscopic probe could possibly be implemented to enable capacitance measurements of internal surface texture, but this is rather unfeasible due to the basic principle behind plate capacitance. Having even accomplished so, the measurement range would still be restricted by the probe length which warrants further development. These two points could be considered as the main deficits to overcome for this technique. It can be culminated that, at present, the technique is not suitable for internal surface testing.

5. Vibration analysis

Vibration parameters are thought to have a correlation with the surface condition. Intuitively, such a phenomenon can be visualized through a wheel rolling through a sinusoidal curved surface, which experiences vibration during the rolling motion. It is evident that through varying the wavelength, amplitude, and superposing other curved surfaces, the wheel's vibration output changes significantly. In general, the rougher the surface, the more sporadic and intense the vibration. From this delta in vibrational behavior, captured through displacements, sound waves or acceleration, a representative roughness value is computed as an indication of the surface texture.

5.1. Rail roughness measurements

An example of such a principle is shown in rail roughness monitoring, in which indirect measurements of rail roughness through accelerometers, microphones, displacement transducers are done and then spectrally analysed. Through one-third octave band processing (Laplace transform and categorizing into third octave bands), and the application of a speed-dependent transfer function [27] to the acceleration data, the total roughness spectrum $L_{tot,eff}$ of the indirectly measured wheel-rail system is obtained. To show the relation of this to the rail roughness, Equation (4) is given below to describe the energy balance for total roughness spectra [27], where $L_{R,rail}$ represents the directly measured rail roughness spectrum, $L_{R,wheel}$ is the directly measured wheel roughness spectrum, and CF refers to the contact filter for calibrating the direct roughness spectra to the coupled wheel-rail spectrum. This equation allows calculation of any one variable given the other three unknowns, hence $L_{R,rail}$ is obtainable through having $L_{tot,eff}$ with given $L_{R,wheel}$ and experimentally defined CF.

$$L_{tot,eff}=\left(L_{R,rail} \oplus L_{R,wheel}\right)+CF \quad (4)$$

Such roughness levels are, however, usually presented in terms of dB in rail roughness contexts $\left(L=20\log\frac{r}{1\mu m}\right)$ [28], where *r* denotes the root-mean-square roughness of the octave band, and plotted against frequency or wavelength values. Note that this is in reference to 1 μm. An example is given in [27], in which the author has given a Figure showing the existence of roughness indication from these dB values, for both rails and wheels. It is to note that the frequency values are computed from f=V/λ, hence the train speed matters and can alter the frequency value even as wavelengths are kept consistent [28]. As the specificity of this method is extremely strong with the use of calibration CF values, in addition to the unconventional roughness values generated, it is hard to extend this rolling-vibration method of roughness measurement unto other applications. The fact that the stylus instrument yields a surface profile with a more straightforward operation also trumps this rolling-vibration method that requires further signal analysis. It is also regrettable that the method is only indicative of roughness and no other surface qualities. Evaluating this under the context of internal surfaces, such a method is unfeasible for obtaining concealed surface data.

5.2. Conventional machining

In the field of conventional machining (*e.g.*, milling, turning), where forms of cutting vibrations are abundant in the process, attempts have been made on correlating the eventual surface quality to these vibration signals that are in terms of displacement and/or force. They are found to have good correlation [29,30]. The main motivation behind these trials is to enable on-line roughness prediction of machined specimens for enhanced productivity through instantaneous feedback. Such techniques typically utilize accelerometers [31-34], acoustic emissions [35,36], or dynamometers [37,38] as sensors in addition to process inputs (feed rate, spindle speed, depth of cut) [39] and employ signal conditioning, modeling techniques as post-processing to predict product roughness. Such post-processing is required as raw vibrational sensor data from machining contains a large amount of noise and is lower in magnitude [39]. Further sophisticated frameworks incorporate multiple sensor types (a sensor-fusion) [40-43] as inputs to algorithms to obtain more comprehensive intel on the roughness result. Cheng *et al.* in [43] showed an example of roughness monitoring setup utilizing sensor fusion to illustrate the practical incorporation of sensors onto a machining equipment. These included acoustic emission, vibration, and cutting force sensors being implemented on a cutting UPM machine.

Benardos and Vosniakos [44] described multiple approaches to roughness prediction in machining processes including: machining theory, empirical investigation, design of experiments (DOE), and artificial intelligence (AI). Among the four discussed, vibrational signals are frequently utilized as either the main or supplementary data of interest for deriving a model for roughness prediction. It is quite clear in these cases however, that the signal post-processing aspect presents more variety over the signal input aspect and is the main differentiator between methodologies presented in literature. Figure 3 summarizes the main post-processing techniques in this field, from the conditioning (time direct analysis, singular

spectrum analysis, Fourier transformations) aspect to the modelling facet (regression, machine learning, response surface modeling).

A time direct analysis refers to statistical analysis (*e.g.* mean, variance) or non-statistical analysis (peak energy, wavelength) of the data without alteration of the signals. On the other hand, Fourier transformation techniques seek to identify features in the spectral domain that are thought to be more closely related to the surface condition. Variations of this occur as attempts at coupling the spectral analysis to the time-domain analysis, in other words, to observe the spectral changes with time. Singular spectrum analysis (SSA) is a robust, non-parametric technique for detaching the noise (unwanted) components of a particular series and then reconstructing the more relevant parts for better signal quality [45]. It works through constructing a matrix from the time-dependent series (the data) which is then subjected to singular value decomposition (SVD) for extracting eigenvalues. A selection of eigenvectors follows as the filtration process before the full series is reconstructed [19, 26]. The difference in the eigenvalue spectrum was also noted to be slightly indicative of the surface texture in [31].

The choice of signal filtering or conditioning is dependent on the raw data and the signal features of interest. A methodology choosing to focus on the correlation between root-mean-squared intensity and the surface output for example, would opt for a statistical analysis of the signals. It is to note that multiple conditioning techniques can be employed at the same time for obtaining the relevant features. These extracted features of interest from signal conditioning are then passed onto the modelling front, of which there are three main methods as shown in Figure 3: regression, machine learning and response surface modeling (RSM). A deep dive into the extended details of machine learning algorithms and other modeling techniques will not be presented here as these far exceed the scope of this review in length and complexity. Guidelines on the selection, applicability, pros and cons of these modeling methods can be found in review papers that are more focused on these topics [26, 30, 31] in the context of machining surface monitoring.

These data-driven methodologies have led to rather accurate results [44], as one would expect, for their specific processes. The main specialty of these methods lies in their capabilities to perform on-line measurements (or predictions) under highly dynamic conditions that would be impossible for other traditional instruments. However, there are two inherent drawbacks to these methods. One, that the overall method requires a large amount of data for establishing and/or calibrating the model, which leads to inapplicability for novel processes or specimens in development as the historical data are simply absent. In the context of machine learning, these data refer to enough training dataset(s). The result of this is that the amount of specimen must be numerous enough to justify the investment into the modeling. Two, that the specificity is extremely strong and hard to generalize, meaning that extending a particular model or methodology to other processes, or the same one of different environmental variables (*e.g.*, specimen material, cutting material, coolant) is probably unviable.

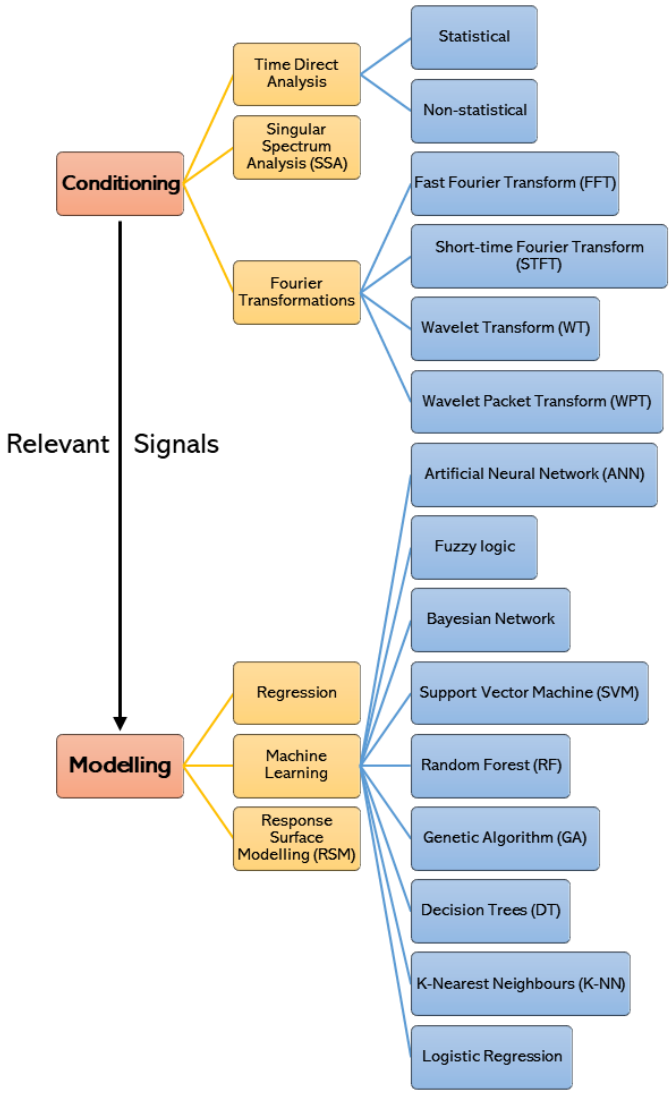

Figure 3. A classification of post-processing techniques in the roughness prediction of machining processes. Information synthesized from [39,44,46].

With respect to applications for internal surfaces, it is unfeasible to try and employ vibrational methods due to the lack of such signals to begin with. To attempt these methods during some part of the manufacturing process (machining, additive manufacturing, extrusion) is likely but even then, the specificity is especially discouraging given the wide-ranging complexity of internal channels with different shapes, sizes, convergence-divergence layouts, and materials. A better takeaway for internal surface measurement from this is the demonstrated capability of machine learning techniques, which could be extended towards utilizing other parameters for internal roughness prediction and characterization.

A possible architecture for this could capitalize on the effects of roughness on pressure, flow rates, and further coupled with the Moody chart for real-time monitoring of internal roughness. Figure 4 shows a simple schematic diagram of this implementation with two pressure sensors (upstream and downstream), and one ultrasonic flow sensor in the middle of a pipe with length L. Knowing the pressure difference ΔP between the upstream and downstream, gives the head loss h over L. And given the flow rate, the average velocity and

hence *Re* (for a Newtonian working fluid) are obtainable. The friction factor *f* can be back calculated from $h = \frac{fLV^2}{D2g}$. Knowing this and the Reynolds number, the relative roughness is then obtainable from the Moody chart. Feeding the sensory inputs to a simple algorithm along with pipe dimensions enables real-time calculation of the internal average surface roughness.

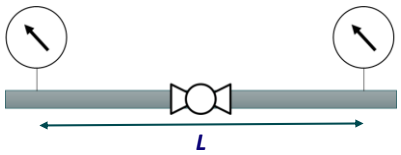

Figure 4. Schematic view of a simple pipe internal roughness monitoring method.

The principle would hold well for a standard circular pipe, but internal channels are largely dissimilar in shape, length, design; and the Darcy-Weisbach equation ($h = \frac{fLV^2}{D2g}$) is unable to fully describe all variations of internal channels. The showcased machine learning methods above would present a promising solution to such a problem. The same schematic applies as in Figure 4, with both an upstream and a downstream pressure sensor for whichever intricate internal channel of interest, flow sensors along the flow direction to obtain an average value of the fluid velocity, and implementing a machine learning algorithm instead of the Darcy-Weisbach equation to model the black box (yet fundamentally existent) relationship between the internal surface roughness and pressure loss, flow velocity. Artificial intelligence (A.I.) have been given particular attention in the fluid dynamics field for applications on feature extraction, flow dynamic modeling, and optimization/control [47]. Neural network methods such as generative adversarial networks (GANs), recurrent neural networks (RNNs) are possible candidates for modeling complex fluid flow problems, and as such, it is not farcical to extend such applications towards roughness monitoring.

6. Optical techniques

The standard methods of NDT mentioned in the introduction involve some limitations in terms of the material and its defects. Firstly, they are sensitive to the physical properties of the material and do not provide any direct way towards measuring the mechanical performances of the material [48]. Moreover, they involve a large amount of time to prepare the sample and to run the process completely. These limitations have led to the recent developments in NDT technology involving optical methods. It promises higher sensitivity with an increase in the detection accuracy by eradicating the complexity involved in the process of signal multiplexing and resistance to electromagnetic interference. It can measure surface deformation or delamination up to a few microns where the types of loading can be vibrational, thermal, vacuum, sound, and pressure *etc.* There are several types of optical NDT technologies such as, laser shearography, endoscopic NDT, infrared thermography NDT *etc.*

6.1. Laser shearography

Laser Shearography is a technique of optical measurement based on laser interferometric phenomenon that utilises the effect of speckle [49]. It is also known as speckle shearing interferometry. A holography related technique known as electronic speckle pattern interferometry (ESPI) is believed to be the origin for this technique [50]. By nature, these techniques are non-contact and can provide a large area measurement which has created an increase in demand for using them in non-destructive testing. Between the two types, shearography has several advantages over ESPI. Shearography is directly sensitive to surface strain, and it can measure the derivative of displacement or the slope whereas ESPI can be used to measure only the displacement of the loaded component's surface. Moreover, as an interferometric technique, the remarkable resilient nature of the shearography process to the disturbances in the environment makes it more suitable for industrial applications [51].

In a laser shearography method, defects and damages of the components' surface are identified when a load is applied to them. The basic principle is based on speckle interferometry. It occurs with the scattering of light from an optically rough surface. The light must possess enough temporal and spatial coherence. The wavelength of the light provided is less than the topographical features of the rough surface. When scattered from different points on the surface, the constructive and destructive interference of light results in the formation of a complex granular pattern. In the nonimage case, laser speckle is known as objective speckle and subjective speckle is achieved when the pattern is imaged [52]. In shearography, the subjective speckle is important because the speckle size can be matched with the resolution of the camera used by selecting the F-number of the imaging lens accordingly.

It records and compares the speckle pattern before and after applying a load on the component under investigation. The test component is first illuminated with a laser and observed through a CCD camera. The camera is equipped with a shearing device [53]. It projects the image of the object on the chip of the camera. The original image of the surface of the unloaded specimen is then recorded. The object is stressed by either type of loading like mechanical, thermal, or acoustic vibrations. The image of the loaded component is then recorded. Due to debonding or delamination, changes in the contour of the surface occur that becomes visible on the display monitor. The display of the video image processed by the computer depicts the defects as bright and dark concentric circles [54]. The bright and dark circles represent constructive and destructive light wave interference, respectively. Thus, the fringe pattern produced by the correlation of the speckle patterns represents the contour map of the measurand. The phase of the correlated fringe pattern is determined by further processing which in turn also improves the fringe contrast and provides quantitative data [55].

The optical configuration of laser shearography arrangement is analysed based on a Michelson interferometer [56]. A speckle pattern is formed when the surface of the test specimen is illuminated by the expanded light from the laser. In the beginning, the scattered light from the surface of the test component arrives at the beam splitter. It is split into two halves. The reference mirror receives half of the light, and the remaining energy moves to the shearing mirror. The shearing mirror is oriented at an angle. The orientation is achieved

by taking the optical axis of the interferometer as a reference. It results in the formation of an image with a lateral shift. The lateral shift takes place with respect to the image formed by the reference mirror.

At the beam splitter, the recombination of the reflected light from the two mirrors takes place, creating the interferometric speckle pattern and subsequently, the pattern is imaged by the camera and displayed by the monitor as shown in Figure 5. Figure 5(a) represents the fringe pattern when an applied shear force is less and Figure 5(b) shows the fringe pattern when the applied shear force is high. Figure 5(c) shows the fringe pattern when filtering is applied after applying high shear force. Figure 5(d) depicts the pattern after demodulation and Figure 5(e) represents the pattern after integration.

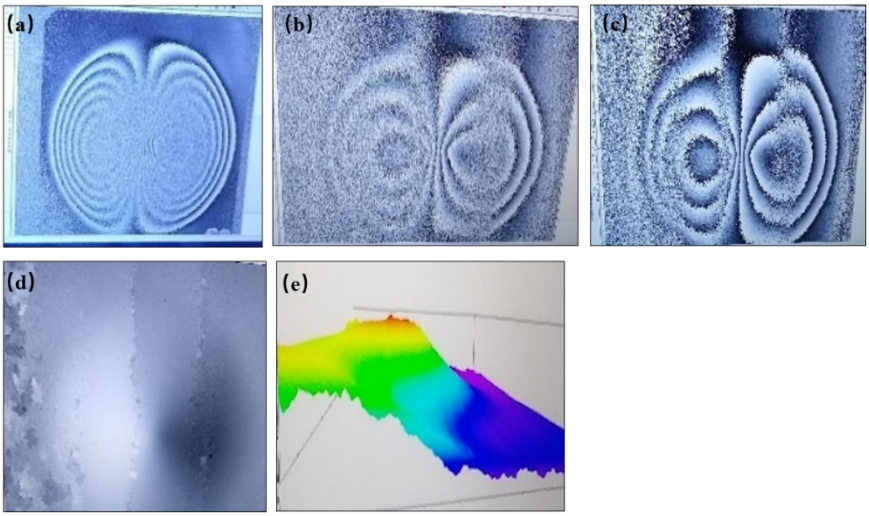

Figure 5. Different patterns of the fringes produced during laser shearography.

The mechanism has been widely applied for rapid inspection of composite structures in production environments [57]. For example, it is applied to avoid potential problems with fatigue and corrosion in the welded structures of the bridge. It is also helpful to critically analyze and provide novel solutions in joining technology for a wide range of aerospace materials and safety-critical applications. In addition, this process is applied in the power generation industries and oil and gas industries to provide structural integrity to various parts and thereby managing the risk mitigation in a broader sense. The rapid nature of the laser shearography process is its main advantage. Moreover, it can execute full-field or large-area measurement. This technique can be applied in evaluating the conditions of the internal surfaces by adjusting the focal length of the negative and the imaging lens depending on the size of the internal surface opening. The focal length of the negative lens may be increased if the length of the internal channel is increased, whereas the focal length of the imaging lens can be reduced while capturing smaller area of the internal surfaces. In addition, the application of subjective speckle may be befitting as the speckle size can be varied depending on the internal surface condition by changing the resolution of the camera and thereby selecting the F-number of the imaging lens accordingly.

Though distinct types of loading like mechanical, thermal, or vibrational can be applied unlike the thermography and ultrasound method, the information regarding the depth of the defect is not directly available with static loading is its main disadvantage. The prominent limitation with this process is that it cannot comply with rigid body motion. In addition, a minimum of three measurement channels are required to make the shearography process fully quantitative along with two orthogonal shear directions which would help interpret all the six components of the surface strain while analyzing the conditions of internal surfaces. The focus could be on the development of shearography instrumentation to investigate dynamic events like rotations, transient vibrations, and shocks.

6.2. Endoscopic NDT

The endoscopy technique for inspecting the quality of an internal surface has been emerging for a few decades. The three main categories evolving under this umbrella are the rod-lens hard endoscopy system, flexible optical-fibre endoscopy system and flexible electron endoscopy. An internal surface can be inspected and analysed by endoscopic NDT that performs optical measurements through a hole. The possible defects in an inner surface can be diagnosed by this technology with extended visual inspection. The mechanism is advantageous as the direction of the sight can arbitrarily altered [58] with minimum damage to the surface of an inspected object [59]. The technology was first applied in medical field in the 1950s and gradually emerged to be a useful technique in maintaining aircraft engine [60].

The working principle of endoscopic NDT involves monitoring of the conditions of internal surfaces by visual methods and then evaluating and diagnosing the optical image. The electronic endoscope is shown in Figure 6 involving features such as light receiving unit, transmission unit and video processing unit that includes video display and image recording. The charge-coupled device (CCD) converts optical signals into digital signals and then the digital signals are further processed by video processing unit for data extraction. In early 1990s, a three-dimensional endoscopic optical system was developed by the US Optical Hybrides company using a “McKinley patent apparatus” [61]. Later in 1998, measurable endoscopic systems, such as IV6C6 endoscopic series and IV8C6 series [62,63] were introduced by the Olympus Corporation. In these systems, the human vision technique was emulated by incorporating dual CCD and thereby the principle of triangulated stereo vision was employed. These were enhanced by merging different technologies that enabled the bending of the probe to 120° for measuring internal diameter of internal surfaces up to 6 mm.

The endoscopy technique is applicable for fault monitoring and diagnosis of the *internal surfaces/parts* of different machine [64]. Continued improvement in the visual features, illumination technique and image resolution of the endoscopy system with charge-coupled device sensors has made this technique more promising in recent years [65]. Automatic endoscopy, 3D endoscopy and in-situ endoscopic NDT are the three realms in which the development has been taken place. For real-time diagnosis of an internal surface, in-situ endoscopic NDT has attracted attention as it creates high application value by saving cost and time.

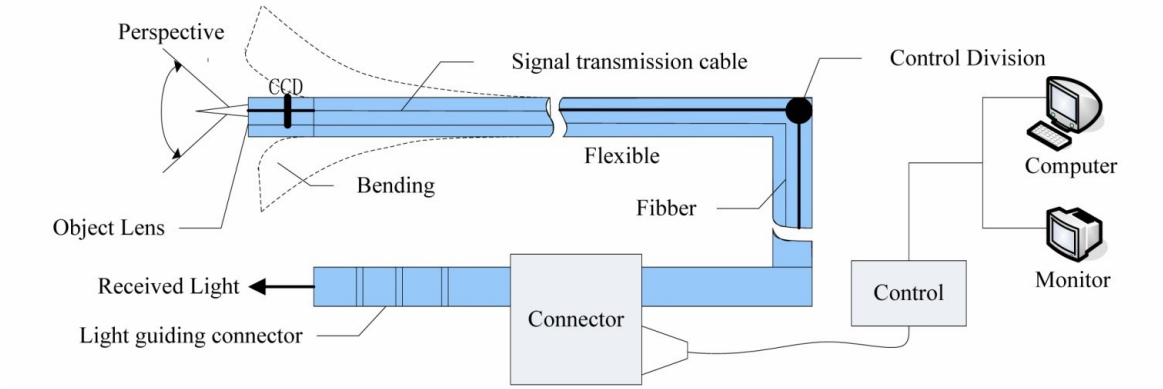

Figure 6. The structure of an electronic endoscope [66]. Copyright© 2011 Zhu *et al.* CC BY 3.0.

6.3. Infrared thermography NDT

IR thermography NDT is a technique to detect the conditions of material's surface by capturing images produced by invisible infrared rays emitted by the surface based on its thermal condition. The technique involves creating a two-dimensional image by converting the spatial variations in infrared radiance from a surface. A range of different colours represent the radiance variance in which warm objects are lighter in colour and cooler objects are darker. Thus, the working principle is based on the temperature difference at different areas on the material surface captured by an infrared camera. Active thermography and passive thermography are the two types of this technique [67] in which active thermography involves a stimulus to heat or cool the target surface whereas passive thermography measures the temperature difference between the target surface and the surrounding environment at different conditions. In addition, based on the heating methods, active thermography has been classified into three categories, such as pulsed thermography (PT), pulse-phase-thermography (PPT), and modulated thermography (MT). A general experimental device is shown in Figure 7 and the results obtained are shown in Figure 8. The technique is advantageous as it is a quick non-contact method that can analyse a large area with real-time measurements.

The evolution of infrared thermography NDT started from 1992 when infrared testing standards have been developed by American Society for Testing and Materials (ASTM) for inspecting and diagnosing the materials conditions used in aircraft industries [68]. Later, an advanced thermography NDT system was built by Inagaki *et al.* [69]. In this system, the test material was kept 500 mm away from the infrared camera. The material surface was covered by a pseudo black body surface. The same material was used to cover the inner boundary layer to keep the inner surface temperature constant as well as to eliminate the multiple reflections between the surfaces. A uniform temperature is maintained inside the system by blowing the air through natural cooling heat exchanger. The surface was heated to a desired temperature by a ceramic heater to find out the defects on it.

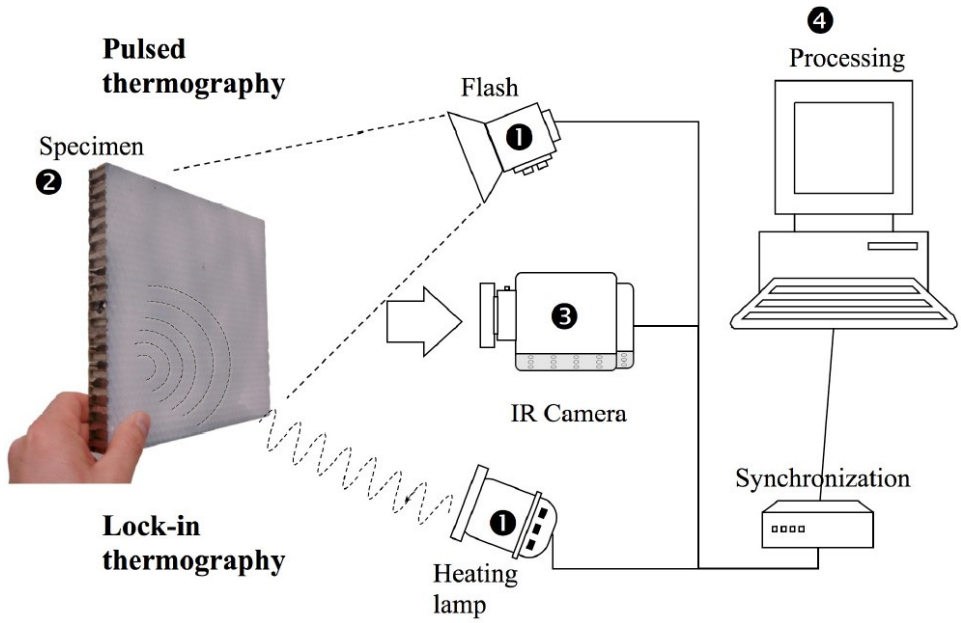

Figure 7. A general device for pulsed thermography and lock-in Infrared thermography NDT technique [67]. Copyright© 2010 Sfarra *et al.* Open access.

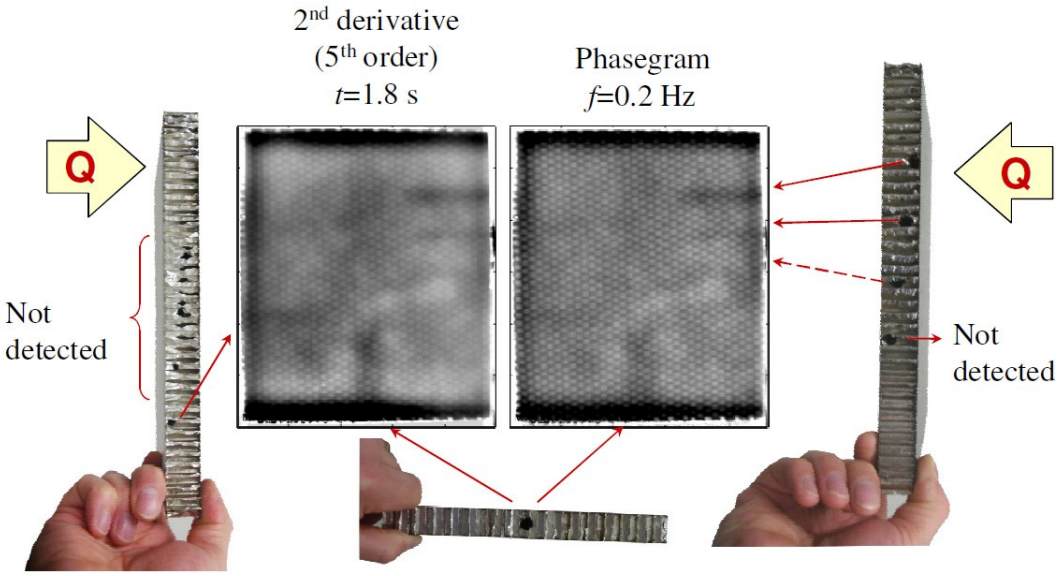

Figure 8. The thermal images of the sample surface [67]. Copyright© 2010 Sfarra *et al.* Open access.

Recently, a pulsed eddy current thermography system [PECTS] has been developed as documented in [70]. An eddy current is induced in the sample under inspection by an induction heating system for a short period and the heat generated on the sample surface is captured by an infra-red camera. The defect on the surface can be visualized from the IR image sequence both during heating and cooling as eddy current density is increased experiencing higher level of heating at the defective zones of the surface. In addition, the

same technique can be applied to study the conditions of the internal surfaces by exposing them to the infrared radiation or pulsed eddy current.

7. X-ray Computed Tomography (XCT)

X-rays are highly penetrative rays [71] on the high frequency end of the electromagnetic spectrum and have seen multiple applications in the fields of engineering, medical science, and even security [72]. The distinctive features of X-rays are their penetrative ability, ionizing capability and atomic-spacing-like wavelengths which have been leveraged in different manners for varying applications, enabling multiple evaluation methods that would otherwise be impossible with visible/ultraviolet light waves.

The penetration ability of X-rays is best illustrated with Figure 9. The extent of electromagnetic radiation penetrating an object is most affected by the density of the object [71], which attenuates the photonic energy of X-rays. Attenuation is also affected by the thickness of the object, and the atomic number of the elements constituting the object. In general, the thicker, the denser the object of higher atomic number, the higher the attenuation effect, quantified as the attenuation coefficient μ. This phenomenon is described by the interaction probability (chance of absorption or scattering) of photons. The concept of photonic ranges (distance travelable before interaction) comes into play here as photons at the same energy level do not have the identical range: it is an exponential distribution (see Figure 10), and generally considered in terms of *average* photonic range [73], equivalent to the reciprocal of the attenuation coefficient (see Equation (5)).

$$\text{Average Range (cm)} = \frac{1}{\mu(\text{cm}^{-1})} \quad (5)$$

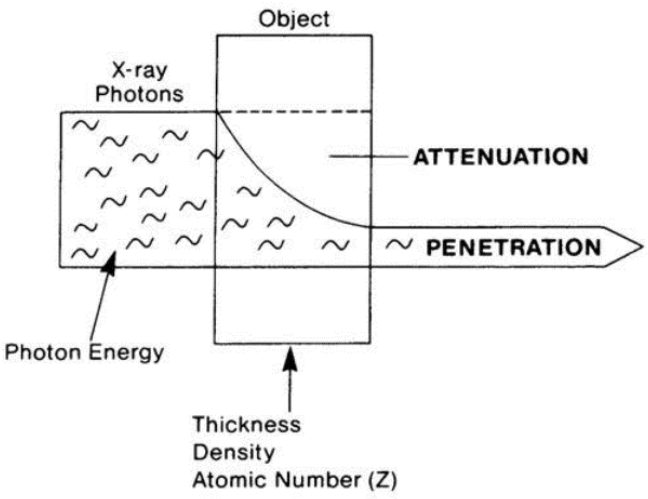

Figure 9. Visualization of the penetration ability of X-rays and attenuation factors [73]. Copyright© 1995 Perry Sprawls and Associates, Inc. Open access.

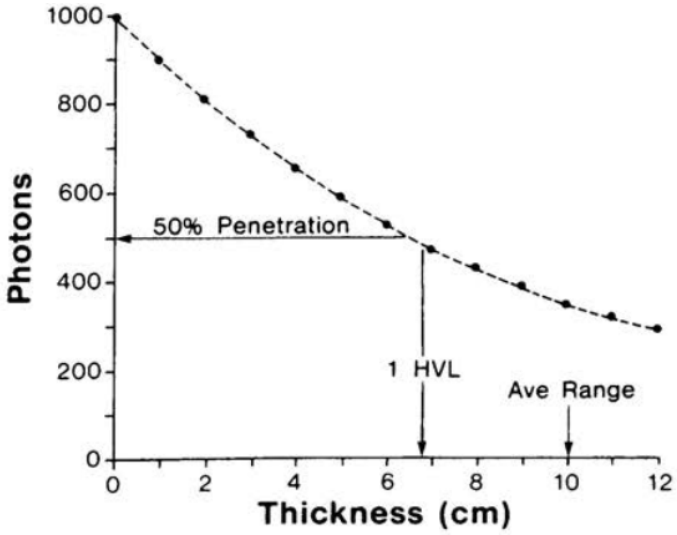

Figure 10. Exponential graph relating the amount of photons to the penetration depth achieved [73]. Copyright© 1995 Perry Sprawls and Associates, Inc. Open access.

It is evident that depending on the density, thickness of the object of interest, the permeability of X-rays varies and yields information in the form of shadows, or 2D X-ray intensity as demonstrated by the X-ray discoverer Röntgen [71] who first showed the skeletal image of a human hand. Marrying this basic principle with computing power is the X-ray computed tomography (XCT) technique which debuted in the field of medical radiology. Introduced by Hounsfield in 1973 [74], an X-ray scan takes numerous 2D scans of a sample from different directions, from which an image reconstruction algorithm computes and creates a 3D image of the internal structures. An example of taking five slices of scan on a sample is shown in Figure 11. The five slices can be thought of as five different snapshots of the sample's cross-sections, which can be recompiled to show a three-dimensional view of the internals. In essence, this recompilation is solving simultaneous equations for the absorption value of each voxel (a 3D equivalent pixel) using the 2D scan readings [74], this is also known as an algebraic reconstruction technique [75]. It is the contrast in the different absorption values generated that allows users to observe features of the internal structure. Modern day XCT instruments, however, commonly employ reconstruction methods such as the filtered back projection, or iterative reconstruction (IR), with artificial intelligence approaches on the rise [76,77]. As the field of computed tomography (CT) itself has a considerable depth, readers are directed to [77] for an excellent illustration on filtered back projection, [75] for more on IR, [76] for a historical perspective, and [78] for mathematical understanding.

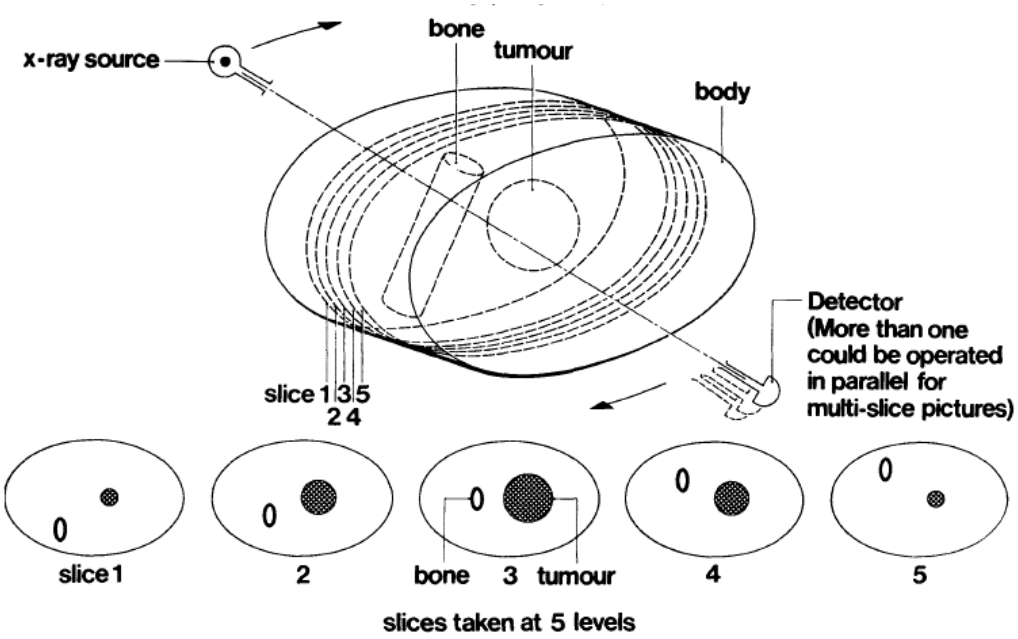

Figure 11. Illustration of five CT scans taken at different slice levels of a sample human body, courtesy of Hounsfield [74]. Copyright© British Institute of Radiology 1973, reprinted with permission.

The image generated is evidently only as good as the contrast conceivable and said contrast could occur from either a change in intensity, or phase shift. These factors are related to the refractive index of the sample n in the sample as given in Equation 6 [77], where β (the imaginary part) is a function of the attenuation coefficient mentioned above, and δ (the real part) is the phase shift. This is a useful phenomenon to exploit when dealing with specimens consisting of low atomic number elements (*e.g.*, carbon) or having internals of similar atomic number (*e.g.*, having copper in a nickel tube), as these show generally poor attenuation contrast, and would benefit from a phase contrast approach to XCT [77].

$$n=1-\delta+i\beta \quad (6)$$

Given XCT's established status as a non-invasive inspection tool for human internals in medical science, it is only natural that attempts have been made to extend XCT onto other fields, including metrology and manufacturing. In a review of XCT applications in additive manufacturing by Thompson *et al.* [79], XCT's extensive usage on porosity analysis through voxel identification was especially highlighted in addition to dimensional analysis for lattices, CAD model validation, and other dimensional measurements. Pyka *et al.* [80] are credited with the pioneering of XCT for surface texture characterization, spawning a series of papers on this topic as noted in [79], which review comments could be summarized as follows: the data resolution is of poor quality as compared to other surface measurement methods, and the surface parameters obtained were about to be "supplanted by other methods of surface metrology"; which presumably, is about areal surface parameters replacing line parameters for A.M. surfaces according to the citation given [81]. Given that line measurements are not

completely phased out, even for A.M. products, this would turn out to be untrue. However, criticisms on Pyka *et al.*'s work are valid: the resolutions are indeed rather poor with 1.5 μm voxel sizes (i.e., 1.5 μm measurement resolution, see Figure 12), the MatLab tool for calculating roughness from the XCT image did not take texture filtration or sampling length into account, as would be standard for line roughness measurements.

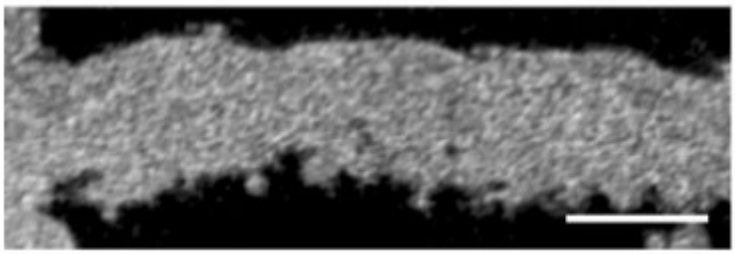

Figure 12. 1.5 μm voxel size micro-CT image of a Ti6Al4V strut with a 200 μm scale bar [82]. Copyright© 2013 WILEY-VCH Verlag GmbH & Co. KGaA. Reprinted with permission.

Although it was an immature method with its flaws for metrology, the development of XCT for surface texture assessment would continue to see progress. Since 2016, many attempts have been made to further efforts on this front. Townsend *et al.* investigated the use of micro-XCT on an A.M. cube for areal texture analysis in comparison to a focus-variation optical instrument, showing a difference of < 2.5% for S_a [83]. However, despite highlighting the non-destructive potential of XCT for evaluating internal surfaces, the specimen chosen in this work was a cube that had no internal surface for assessment. In a similar fashion, Zanini *et al.* attempted to characterize A.M. surface (a sample cube) with a generalized surface parameter measured with XCT, and noted the discrepancy to the conventional line parameters whilst concluding that XCT provides better surface depiction as compared to optical instruments [84]. Thompson *et al.* measured the surface texture of a concealed surface specimen (simulating the inaccessibility of internal surfaces) with two XCT machines, and compared the results with optical instruments (focus variation microscope, coherence scanning interferometry), showing rather promising results (see Figure 13) despite having voxel sizes of 5.7 μm and 5.0 μm [85].

Kantzos *et al.* [86] utilized a *synchrotron* X-ray source for CT scanning a 1 mm^2 Ti6Al4V A.M. surface sample with a 0.65 μm/voxel resolution, producing images with minimum feature resolution of nearly 1.5 μm (likely the highest yet), with clearly identifiable surface features. It is regrettable that the sample had to be "extracted" from the surface for fitting in the XCT instrument, and could not be used for assessing a concealed surface, due to constraints on the specimen size. However, the XCT-micromechanical modeling methodology was shown to be a possibly effective evaluation of A.M. surfaces, capable of capturing detail beyond conventional surface measurement methods.

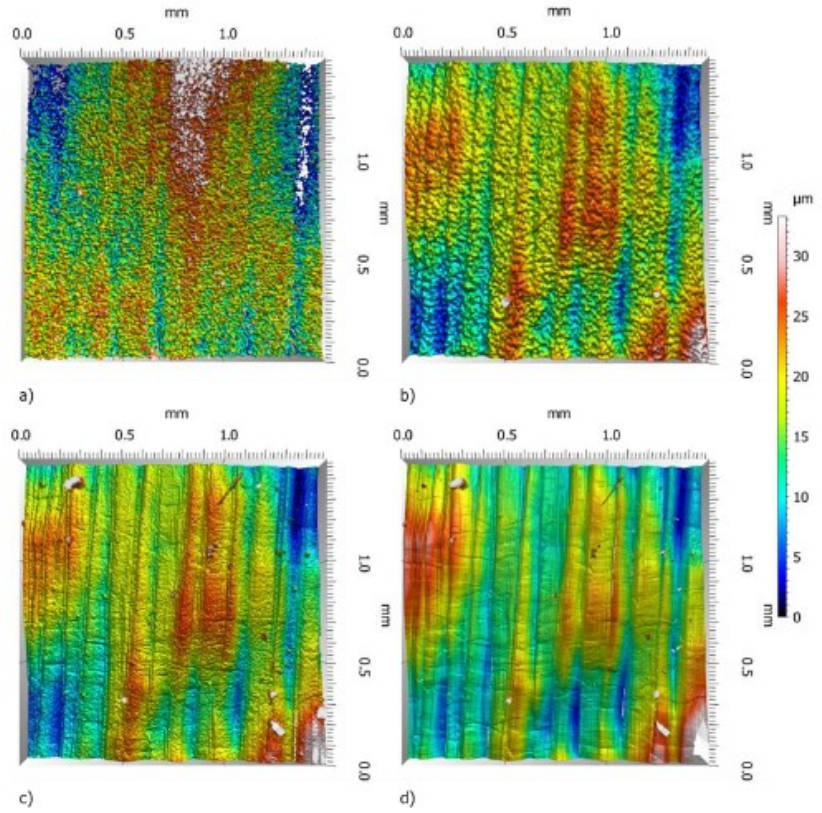

Figure 13. Surface topography maps (levelled) of: **(a)** Zeiss XRadia XCT (5.75x geometric magnification, 0.4x optical magnification); **(b)** Nikon XCT (35x geometric magnification); **(c)** focus variation device (20x objective lens, ring light); **(d)** confocal scanning interferometry (20x objective lens, no zoom); XRadia XCT shows dissimilarity due to having the most noise [85]. Copyright© 2017 Thompson *et al.* CC BY 4.0.

Klingaa *et al.* [87] implemented an in-house Python-based methodology towards assessing the R_a of A.M. channels of different build orientations with XCT at a voxel size of 15.9 µm. The processed 3D deviation data was used to generate profile data. The R_a was then calculated according to ISO 4287:1997 standards, but it was explicitly stated that sampling length and evaluation length were not strictly followed, instead, the program performed a leveling of the profile and then removed the least-squares-fitted-line from the profile, presumably as a substitute for cutoff filter. The authors have also provided bottom-up profiles showing clear signs of surface texture indication in their work. Said R_a values were not compared, however, to other instruments of surface inspection, hence it is impossible to compare the efficacy or accuracy to the commonly known standards. Regardless, the research work shows good potential of XCT for internal surface assessment, given the 3D profile information that is reasonably well-computed for visualization as well as analysis. As an extended study, Klingaa *et al.* implemented a similar methodology towards characterizing geometry and surface texture of laser powder bed fusion manufactured aluminum channels in 2021 [88]. They found that the voxel size has a stronger quantitative (surface texture parameter) effect than a qualitative effect, such that a qualitative evaluation (visual inspection and illustration applications) may not require fine resolution of small features. Furthermore,

they evaluated multiple surface line parameters, and debated the appropriateness, interchangeability of such parameters for certain goals, *e.g.*, surface texture as a function of local angular orientation was found to be quantifiable through P_a, $P10_z$, and P_q. The line texture parameters were evaluated with sampling length of 4.5 mm, but were not compared to other methods of surface evaluation. Regardless, the authors have showcased good capabilities of internal surface inspection through XCT and their Python texture assessment code.

In an earlier work in 2019, Klingaa *et al.* had applied XCT to A.M. helical curvy cooling channels [89], with results output in the form of surface texture parameters (as opposed to line parameters). Figure 14 shows a portion of the reconstructed image. Once again, the outputs were not compared to other instruments, but surface parameters are likely to be more appropriate for a curved surface as per the authors' specimen, and the reality is that no other instruments are fully capable of measuring curved surfaces to serve as a basis of reference. They found that the estimated texture agreed with problems commonly known to powder bed fusion in constructing overhanging portions of a part, and further concluded that the proposed methodology was possible for internal surface characterization, if issues with resolution could be solved.

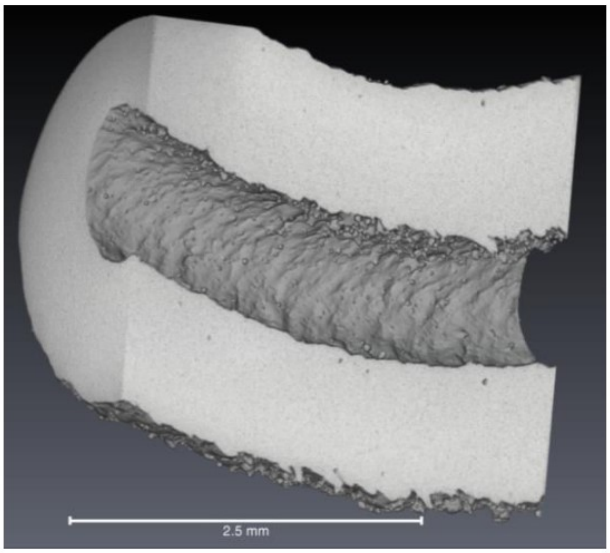

Figure 14. A section of the reconstructed image from XCT of the helical channel [89]. Copyright© 2019 Klingaa *et al.* CC BY 4.0.

Fox *et al.* investigated the use of XCT in complement with confocal microscopy for surface finish and defect detection of A.M. samples; they noted the low-resolution limitation of XCT that restricts surface topography analysis [90]. In the study, a voxel interpolation technique was also employed in hopes of obtaining higher reconstruction quality, but it was shown to provide little improvement. Evsevleev *et al.* trialed the usage of XCT on various quantitative analyses of Triply Periodic Minimal Surface Structures (TPMSS), including a surface roughness analysis section [91]. The surface analysis situation here is alike that of an internal surface one, as interior textures of the lattice are concealed behind multiple repeating

layers (see Figure 15). The roughness profile was obtained through calculating the distance between the original and low pass filtered (smoothened to be indicative of the baseline shape) profiles. Figure 16(a) shows the original profile *versus* the filtered profile, Figure 16(b) shows the original profile (black), the filtered profile (continuous red line), the distance between them and the eventual roughness profile yielded.

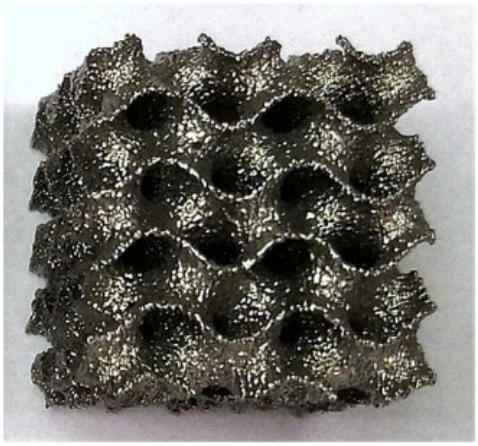

Figure 15. A TPMSS specimen with 0.4 mm wall thickness [91]. Copyright© 2021 Evsevleev *et al.* CC BY 4.0.

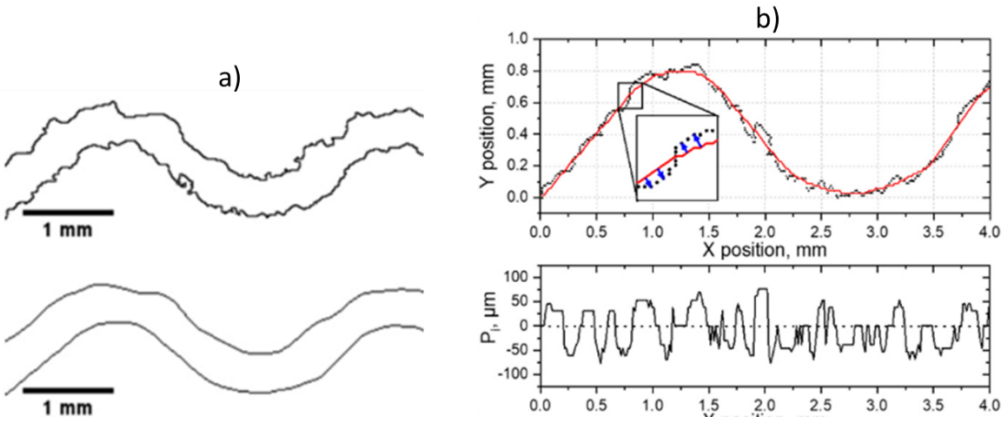

Figure 16. Surface roughness measurement methodology [91]. **(a)** The original vs filtered profile; **(b)** illustrating the distance calculation between original and filtered profile, and the roughness profile as a product. Copyright© 2021 Evsevleev *et al.* CC BY 4.0.

The arithmetic mean was then taken and found to be within the range of similarly manufactured samples in literature (< 40 µm). Zanini *et al.* investigated a method of accuracy verification for XCT surface topography measurements in [92], noting that high-resolution XCT could attain surface profiles and re-entrant features with minimal deviation to the reference. On the other hand, focus variation (FV) and confocal microscopy (CM) techniques were found to be inadequate in obtaining concealed features such as prominent undercuts.

To illustrate the suitability of XCT further, a case study by Lifton *et al.* in 2022 [93] demonstrated the feasibility of XCT surface roughness measurement on an A.M. internal channel. The raw XCT scan had a voxel size of 0.04 mm, and was reconstructed using

manufacturer software (Nikon). Surface characterization was performed through measuring the 3D mean deviation from a standardized cylinder in a digital software (GOM Inspect) to illustrate the effects of Abrasive Flow Machining (AFM) on internal surface texture (see Figure 17). It is evident that detailed internal surface information is obtainable from XCT, and that it can qualitatively, quantitatively (to a certain extent) showcase roughness differences, although the accuracy of measurements in this study has yet to see verifications from other methods.

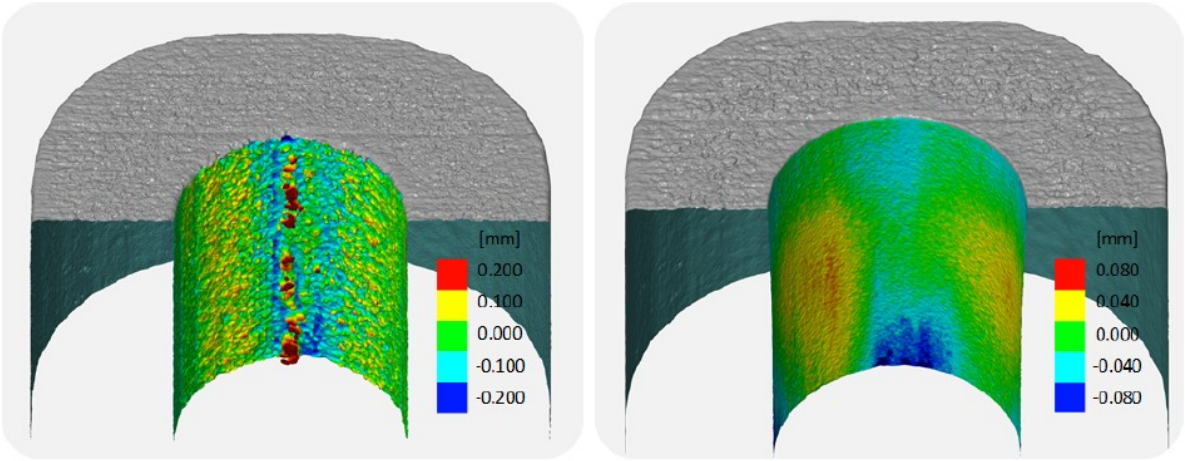

Figure 17. XCT scan results of the downskin surface pre- (left) and post- (right) AFM processing [93]. Contour colors designate deviations from the fitted cylinder.

Clearly, XCT has a huge advantage in the scene of internal surface assessment, in terms of accessibility and its non-destructive nature, enough to see substantial research work in this aspect. The greatest hindrance to XCT adoption so far is the problem of resolution. To observe the features upon a surface would require imaging voxel sizes to be at least smaller than the features itself, and in the realm of surfaces, this equates to an almost micrometer or sub-micrometer range. In compliance to the underlying principles of image reconstruction, a sample's entire cross-section must be irradiated and be within the field of view (FOV) of the detector(s) for all the scans, this means that a better XCT resolution (smaller voxel size) inevitably allows only a smaller sample size for measurement [77]. Stitching methods alike the ones used for optical microscope devices could be applied for combining multiple FOVs of different sections, but it is plain that the data storage and reconstruction time requirements increase heavily as a result of high-resolution stitching [77]. Scan times could also be an issue when voxel size/actual size ratios are incredibly low, as too large an angular change would not provide enough imaging data for a faithful reconstruction. As such, intricate features tend to be more difficult to detect on a larger part than a smaller part [79].

Further limitations in this application are in the form of: enclosing material thickness [94], where the surrounding attenuation coefficient heavily affects the encapsulated surface's obtainable information; imaging artefacts [77], which are deviations from the true attenuation factors of the sample owing to varying factors; and dosage concerns, primarily in the cases

of synchrotron X-ray sources (high energy, high flux applications) [77] causing photoelectric effects, fluorescence, or heat effects. In addition, material porosity and sharp edge effects could also hinder imaging qualities and lead to extra errors. Nevertheless, as duly noted in [89], the measurement of curved internal surfaces is currently only possible by XCT, and to produce similar results using other methods, would require an extraordinary amount of effort into specimen slicing, algorithmic levelling, or probe adjustments. This fact alone substantiates the unique strength of XCT for concealed surface assessment despite some limitations in the method. Novel scanning methodologies, image reconstruction algorithms, machine learning approaches [76,77,95], are all efforts towards realizing fast, high-resolution XCT that could enable it for internal measurements.

8. Replica methods

Replication is used to copy the surfaces and the replicas are brought to the measuring device for measurement. The technique has been widely researched and exploited in the medical and dentistry fields for replication of skin texture, and tooth. The emphasis here is limited to usage of the technique in manufacturing related surface measurement studies. The process is employed to quantify surface finish in cases where measurement instruments cannot access some surfaces (difficult-to-access areas) [96] to evaluate them directly, and/or when the part to be measured is too heavy or too large or cannot be dismantled to be brought to a measurement instrument. A setting compound is poured onto the area of interest; when it has been cured it can be removed, thus providing a solid surface which ideally should be identical with the area of interest [97]. A replica will be the inverted profile of that of the surface of interest (see Figure 18).

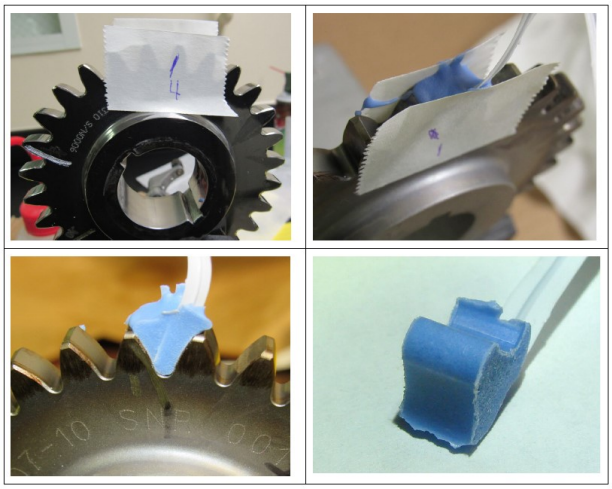

Figure 18. From [98], showing hard epoxy replication process. Copyright© 2019 American Gear Manufacturers Association (Reprinted with permission).

The accuracy of the replication, including replication materials and replication methods, is critical in actual applications [96]. Different replication materials and methods have different replication performance. In this section some of the existing work studying in-depth

the accuracy of various replication materials and methods will be looked at. The different replication materials experimented on and studied in the works below are presented in a consolidated and summarized manner in Table 1 for easy grasp and better understanding. Some other highlights from the studies will be discussed below.

George A.F. compared 4 various replica materials and techniques using power spectral density function, fidelity analysis and concluded that for surface replication, a quick-setting material is enough when analyzing surface roughness alone [97]. Time consuming techniques and a less convenient system are required when surface shape is also required in addition to surface roughness. The work also emphasized how shape of replica affects its fracture on release, lifter geometries and use of releasing agents to remove replicas without any damage to both replica and mold. The dimensional features and surface topographies of the mold are directly transferred to replicated products. The mold surface can directly affect the replication process since it influences, for instance, demolding forces [99].

James *et al.* investigated replicating qualities of two resin systems containing inorganic filler powders and found that the highest standard of replication was achieved using slate powder and mica flour. Shrinkage levels were reposted to be significantly low when compared to unfilled systems [100]. Nilsson *et al.* had done a comprehensive study of three different materials- Araldite, MicroSet and Technovit, for surface roughness replication on five different types of machined surfaces - steel sheets (electron beam texturing and shot blasted texturing), a cylinder liner, a crankshaft and a face-ground surface and concluded that accuracy of these replicas is within 10% and the repeatability is better than 10% (excluding S_z) [101]. In a study by Liu *et al.* the replica materials, Repliset, Technovit and Press-O-Film, have been used to replicate four ground surfaces with average roughness values in the range 0.2 µm, 0.4 µm, 0.8 µm, and 1.6 µm. Surface average roughness was calculated and compared between the original surfaces and their replicas [96].

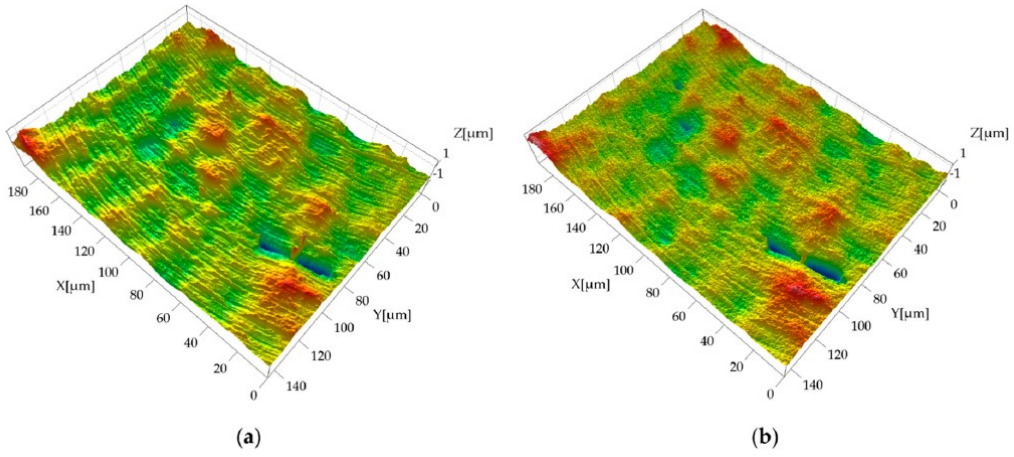

Figure 19. From [99], (**a**) metal master; and (**b**) silicone replica. The original silicone acquisition was inverted with respect to the x- and z-axes to facilitate the visual comparison. Copyright© 2017 Baruffi *et al.* CC BY 3.0.

Baruffi *et al.* have presented a comprehensive and detailed knowledge on application of replica molding technique to micro milled surfaces and geometries. They evaluated the performance of RepliSet and concluded the indirect and direct measurements provided the same results in 34 cases out of 36, demonstrating that it was suitable for characterizing micro milled surfaces that are inaccessible for other measurement systems [102]. Surface topography captured by optical method of the master mold and the replica is shown in Figure 19. To accurately replicate the surface texture of archaeological materials for surface metrology measurements, two more molding compounds (Affinis, Povil novo) were tested and reported in [103]. Matthew Bagner *et al.* in [98] have demonstrated replication of a gear tooth profile using Repliset and a hard epoxy resin (Facsimile) and both showed high replication quality that was analyzed through fidelity analysis. To know more about fidelity analysis, readers are referred to [98].

Table 1. Consolidated and summarized Replication materials from the mentioned references.

S.No.	Material	Reference	Description/Mixture	Remarks	Soft/Hard Resin	Setting Time
1	Acrulite Microtech Type A	[97]	Polymethylmethacrylate Resin	Specially developed for surface replication; Bowing can occur and information becomes less reliable if wavelength increases.	Hard	20 min
2	Araldite	[97], [101]	Two component Epoxy Resin; 1. Araldite CY219 2. Mixed with 40% Aluminium Powder Filler 3. Araldite SV40	Used in Casting and Lamination purposes; Brittle Replicas; Suitable for surfaces with fine textures.	Hard	1 day, 3 days, 1 day
3	Strand Glassfibre Resin	[97]	Polyester Resin–4 types	Used in glass fiber applications; Brittle and leaves residue on surface.	Hard	30–60 min
4	Polymaster	[97]	Polyester Casting Resin		Hard	
5	MY 753/HY 951 resin	[100]	Resin/Hardener mixed in a 100:10 ratio by weight. Fillers: 1. Slate Powder 2. Mica Flour 3. Silica Flour Marble Flour	Slate powder and Mica flour filler powders with that have high specific surface area resulted in higher standard of replication.	Hard	24 hr

Table 1. *Cont.*

S.No.	Material	Reference	Description/Mixture	Remarks	Soft/Hard Resin	Setting Time
6	CY 219/HY 219/DY 219 resin	[100]	Resin/Hardener/Accelerator mixed on a 100:50:5 parts ratio by weight. Fillers: 1. Slate Powder 2. Mica Flour 3. Silica Flour 4. Marble Flour	Minimal level of down to 0.11% linear shrinkage.	Hard	24 hr
7	Technovit	[101], [104]	Two-component cold-curing resin based on methylmethacrylate; Replica Liquid/Powder in the ratio 3:1	Specifically made for roughness replication on fine surfaces; Silicone release agent to be applied on surface before pouring resin to aid easy removal of the replica; Requires building a containment wall around the area to be replicated and the replication should be done in fume hood with proper equipment.	Hard	15 min
8	Microset 101 RF	[101]		Elastic; Suitable for small and deep holes; They show lower surface parameter values than the original.	Soft	20 min
9	RepliSet	[104], [99], [98]	Polymer + Curing agent	High accuracy in replicating surfaces with Ra ranging from 0.4 µm to 1.6 µm for roughness measurement rather than smooth surfaces with Ra 0.2 µm.	Soft	5 min

Table 1. *Cont.*

S.No.	Material	Reference	Description/Mixture	Remarks	Soft/Hard Resin	Setting Time
10	Press-O-Film	[104]	Layer of compressible micro-foam coated onto an incompressible polyester substrate	Burnishing quality, *i.e.*, force applied on to the film affects replication accuracy significantly.	Soft	30 sec Burnishing
11	Affinis	[103]	Viscosity: 1. Light body 2. Heavy body	Resins used in surface metrology analysis of objects of varied sizes in archeological study.	Soft	2 min, 2 min
12	Povil Novo	[103]	Viscosity: 1. Light body Medium body	Resins used in surface metrology analysis of objects of varied sizes in archeological study.	Soft	3.5 min, 2.5 min
13	Facsimile	[98]	Casting Liquid/Powder in the ratio 3:1, mix for 35-40 seconds forming no lumps	To rapidly remove replicas, cooling the specimen will help.	Hard	30 min

8.1. Replica tape reader

Replica tape is a relatively inexpensive, simple method of surface profile replication. This method also works on curved surfaces and has the option of retaining a physical replica of the surface. The test method conforms to ASTM D4417-C and ISO 8503-5. Replica tape consists of an incompressible polyester substrate of uniform thickness that is coated with a layer of compressible micro foam (Example: Press-O-Film). When collapsed against a surface, the foam acquires an impression of the surface "profile", such that the highest peaks on the original surface come to rest against the polyester layer and the deepest valleys are replicated as peaks in the foam (Refer to Figure 20). Subtracting the thickness of the incompressible substrate from the resulting replica gives a good measure of peak-to-valley height of the profile.

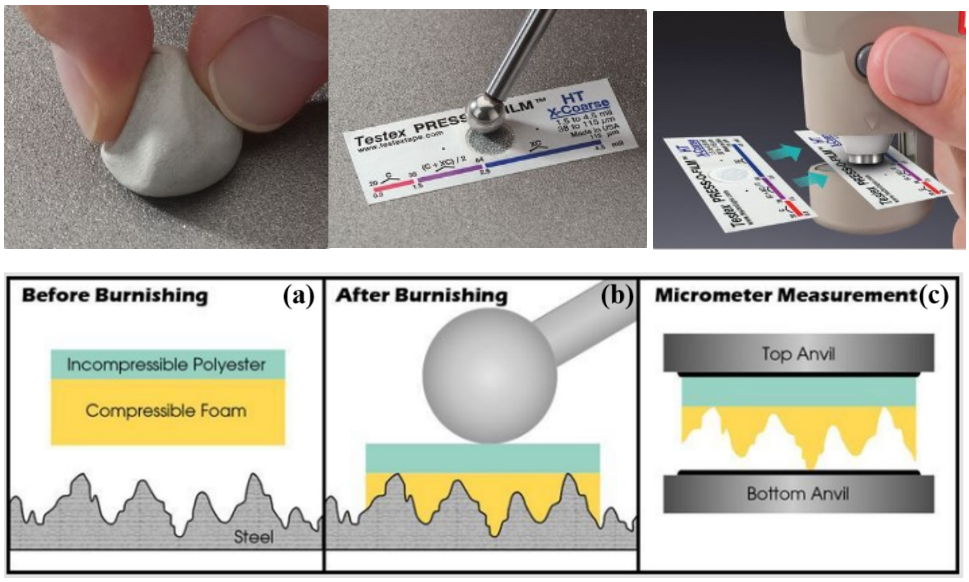

Figure 20. From [105], **(a)** Using Cleaning putty to remove dust, debris, or residual blast media from the measurement site; **(b)** Burnishing using burnishing tool; **(c)** Measurement using Digital Tape reader. Reprinted with permission from Defelsko Corporation. Copyright© 2023 Defelsko Corporation (Reprinted with permission).

Replica tape, in wide-spread and long-standing use to assess surface profile in the coatings and linings industry, displays a somewhat non-linear replication response to roughness. Digital processors like Positector [105] can be used to compensate for non-linear sensor response and are commonly used for this purpose in modern measurement devices. Refer to article [106] for procedures that can be used to linearize roughness measurements made with replica tape. A separate response curve is deduced for each grade, or thickness, of replica tape. Replica tape measurements of the surface roughness on silcrete artefacts were used in [107] to evaluate the quality of visual classification of heat-treated *vs.* not-heated artefacts. It was reported that replica tape measurements were a promising alternative to visual classification independent of any observer's bias unlike the latter.

The quality of replication depends on the time available for the curing process and the acceptable level of inconvenience (due to mixing and handling) [97]. Materials that are elastic like Microset can be used for deep internal channels. Also, soft resins that are easy to remove after replication can be used for small holes and blind holes. There is research gap in studying usage of replica tape for internal surface measurement, reason being, even though the tape can reach surfaces in deep, oblique channels, there will be hindrance in burnishing and difficulty in removing the tape without damage. The method is completely off-line which is a drawback since in-process surface monitoring is out of scope.

9. Conclusion

Discussions of various surface measurement methods drawing from different principles have been shown in this paper, with clear indications of methodologies, techniques that could be suitable for extension towards non-destructive internal surface assessment. The rather

commonly used, traditional measurement methods of stylus and various microscopies are quite evidently not well-equipped for such purposes. Diving into capacitance methods, it was found that though it showed potential for rough estimations of the surface roughness condition, and could be viable for on-line dynamic measurements, the techniques developed are heavily skewed towards external plane surfaces. They require further developments in advancements of probe flexibility, extensibility before consideration for internal surface measuring. Vibration analysis showed niche purposes not extensible beyond their fields, but the artificial intelligence aspects proved to be a strong tool for prediction, and a fluid-mechanics-based framework leveraging on this aspect was proposed as a candidate for internal measurements. Optical techniques have demonstrated their feasibility on general surfaces, but endoscopic NDTs prove to be the most promising methods for this intention. Shearography and infrared thermography face difficulties in the detector side of equipment and require further advancements on detector miniaturization and integration for enabling such applications.

Among the discussed techniques, XCT is a clear favorite for internal surface assessment with its unique penetration capability, with multiple variations of applications demonstrated in literature, but resolution improvements are still required. This could be realized through better reconstruction algorithms, novel scanning methodologies, or improved X-ray energy sources. Replica methods are, surprisingly, shown to be a rather strong contender for this application, but are described to not be completely undisruptive due to tape residue and adhesive problems. They are also unsuitable for in-process measurements of any kind.

Bearing in mind XCT's resolution issues, and that high-frequency in-process measurements almost certainly require synchrotron sources (which are rare in the world), XCT would still appear to be the best method for internal assessment. Unlike other methods that do not have the capabilities at all, XCT has the characteristics that await development for unlocking further potential, in addition to already having some feasibility proofs in literature. It can therefore be surmised that XCT is likely to be, at present, the best approach towards fulfilling requirements of internal surface measurement.

Acknowledgements

This research work has been performed under ManTech Project 1.1 at Rolls-Royce@NTU Corporate Laboratory, School of Mechanical & Aerospace Engineering, NTU, Singapore, with support from the National Research Foundation (NRF) Singapore under the Corp Lab@University Scheme.

Authors' contribution

K.Z. Teh: Conceptualization, Data Curation, Formal Analysis, Investigation, Methodology, Software, Visualization, Writing–Original Draft, Writing–Review & Editing; Saikat Medya: Data Curation, Formal Analysis, Investigation, Resources, Visualization, Writing–Original Draft; Sugandhana Shanmuganathan: Data Curation, Formal Analysis, Investigation,

Visualization, Writing–Original Draft; S.H. Yeo: Funding Acquisition, Supervision, Validation, Writing–Review & Editing.

Conflicts of interest

The authors declare no conflict of interest.

References

[1] Ngo TD, Kashani A, Imbalzano G, Nguyen KTQ, Hui D. Additive manufacturing (3D printing): A review of materials, methods, applications and challenges. *Composites Part B* 2018, 143:172-196.

[2] Kadivar M, Tormey D, McGranaghan G. A review on turbulent flow over rough surfaces: Fundamentals and theories. *Int. J. Thermofluids* 2021, 10.

[3] Greitemeier D, Dalle Donne C, Syassen F, Eufinger J, Melz T. Effect of surface roughness on fatigue performance of additive manufactured Ti–6Al–4V. *Mater. Sci. Technol.* 2015, 30(7): 629-634.

[4] Xiao NH. New Technologies and Technical Standards for Modern Non-Destructive Testing Technology and Application. *Beijing: Beijing Silver Sound Audiovisual Press*, 2004.

[5] McCann DM, Forde MC. Review of NDT methods in the assessment of concrete and masonry structures. *NDT&E Int.* 2001, 48:71-84.

[6] Shen GT. Insight - Non-Destructive Testing and Condition Monitoring. 2006, 48(7): 398-401.

[7] Ostash O, Andreiko I, Holovatyuk Y. Degradation of materials and fatigue durability of aircraft constructions after long-term operation. *Mater. Sci.* 2006, 42(4): 427-439.

[8] Abbott EJ, Firestone F. Specifying surface quality. *Mech. Eng* 55:569.

[9] Jiang X, Scott PJ, Whitehouse DJ, Blunt L. Paradigm shifts in surface metrology. Part I. Historical philosophy. *Proc. R. Soc. A.* 2007: 2049–2070.

[10] Taylor Hobson/ AMETEK. The Taylor Hobson Story. *History*. Available on: https://www.taylor-hobson.com/aboutus/history (accessed Apr. 24, 2023).

[11] Davies H. The reflection of electromagnetic waves from a rough surface. *Proceedings of the IEE-Part IV: Institution Monographs*, 1954, 101(7): 209-214.

[12] Birkebak RC. Monochromatic Directional Distribution of Reflected Thermal Radiation from Roughened Surfaces. The University of Minnesota, Michigan, 1962.

[13] Sprague RA. Surface Roughness Measurement Using White Light Speckle. *Appl. Opt.* 1972, 11(12).

[14] Whitefield RJ. Noncontact optical profilometer. *Appl. Opt.* 1975, 14(10): 2480-2485.

[15] Binnig G, Rohrer H. Scanning Tunneling Microscopy. *Surf. Sci.* 1983, 126: 236–244.

[16] Binnig G, Quate CF, Gerber Ch. Atomic Force Microscope. *Phys. Rev. Lett.* 56: 930-933.

[17] Jiang X, Scott PJ, Whitehouse DJ, Blunt L. "Paradigm shifts in surface metrology. Part II. The current shift," *Proc. R. Soc. A.* 2007, 463: 2071–2099.

[18] Murugarajan A, Samuel GL. Measurement, modeling and evaluation of surface parameter using capacitive-sensor-based measurement system. *Metrol. Meas. Syst.* 2011, 18(3): 403-418.

[19] Garbini JL, Koh SP, Jorgensen JE, Ramulu M. Surface Profile Measurement During Turning Using Fringe-Field Capacitive Profilometry. *Journal of Dynamic Systems, Measurement, and Control* 1992, 114(2): 234-243.

[20] Mathiyazhagan R, SampathKumar S, Karthikeyan P. Estimation of Surface Roughness on Milled Surface Using Capacitance Sensor Based Micro Gantry System through Single-Shot Approach. *Micromachines* 2022, 13(10).
[21] Mathiyazhagan R, Sampathkumar S, Muthuramalingam T. Prediction Modeling of Surface Roughness Using Capacitive Sensing Technique in Machining Process. *IEEE Sensors Journal* 2019, 19(21): 9997-10002.
[22] Gao W, *et al.* On-machine and in-process surface metrology for precision manufacturing. *CIRP Annals* 2019, 68(2): 843-866.
[23] Nowicki B, Jarkiewicz A. The in-process surface roughness measurement using fringe field capacitive (FFC) method. *Int. J. Mach. Tools Manuf.* 1998, 38(5): 725-732.
[24] Maize K, Mi Y, Cakmak M, Shakouri A. Real-Time Metrology for Roll-to-Roll and Advanced Inline Manufacturing: A Review. *Adv. Mater. Technol.* 2023, 8(2): 2200173.
[25] Garbini JL, Saunders RA, Jorgensen JE. In-process drilled hole inspection for aerospace applications. *Precis. Eng.* 1991, 13(2): 125-134.
[26] Tian GY, Zhao ZX, Baines RW, Corcoran P. A miniaturised sensor for deep hole diameter measurement. *Precis. Eng.* 1999, 23(4): 236-242.
[27] Verheijen E. A survey on roughness measurements. *J. Sound Vib.* 2006, 293(3-5): 784-794.
[28] Thompson DJ. On The Relationship Between Wheel And Rail Surface Roughness And Rolling Noise. *J. Sound Vib.* 1995, 193(1): 149-160.
[29] Jang DY, Choi YG, Kim HG, Hsiao A. Study of the correlation between surface roughness and cutting vibrations to develop an on-line roughness measuring technique in hard turning. *Int. J. Mach. Tools Manuf.* 1996, 36(4): 453-464.
[30] Wang H, To S, Chan CY. Investigation on the influence of tool-tip vibration on surface roughness and its representative measurement in ultra-precision diamond turning. *Int. J. Mach. Tools Manuf.* 2013, 69: 20-29.
[31] Salgado DR, Alonso FJ, Cambero I, Marcelo A. In-process surface roughness prediction system using cutting vibrations in turning. *Int. J. Adv. Manuf. Technol.* 2009, 43: 40-51.
[32] Khorasani A, Yazdi MRS. Development of a dynamic surface roughness monitoring system based on artificial neural networks (ANN) in milling operation. *Int. J. Adv. Manuf. Technol.* 2017, 93: 141-151.
[33] Lin SC, Chang MF. A study on the effects of vibrations on the surface finish using a surface topography simulation model for turning. *Int. J. Mach. Tools Manuf.* 1998, 38: 763-782.
[34] Plaza EG, López PJN. Surface roughness monitoring by singular spectrum analysis of vibration signals. *Mech Syst Signal Process* 2017, 84: 516-530.
[35] Diniz AE, Liu JJ, Dornfeld DA. Correlating tool life, tool wear and surface roughness by monitoring acoustic emission in finish turning. *Wear* 1992. 152: 395-407.
[36] Reddy TS, Reddy CE. Real Time Monitoring of Surface Roughness by Acoustic Emissions in CNC Turning. *J. Eng. Sci. Technol. Rev.* 2010, 3(1): 111-115.
[37] Risbood KA, Dixit US, Sahasrabudhe AD. Prediction of surface roughness and dimensional deviation by measuring cutting forces and vibrations in turning process. *J. Mater. Process. Technol.* 132: 203–214.
[38] Huang B, Chen JC. An In-Process Neural Network-Based Surface Roughness Prediction (INN-SRP) System Using a Dynamometer in End Milling Operations. *Int. J. Adv. Manuf. Technol* 2003, 21(5): 339-347.
[39] Manjunath K, Tewary S, Khatri N, Cheng K. Monitoring and Predicting the Surface Generation and Surface Roughness in Ultraprecision Machining: A Critical Review. *Machines* 2021, 9(369).

[40] Azouzi R, Guillot M. On-line prediction of surface finish and dimensional deviation in turning using neural network based sensor fusion. *Int. J. Mach. Tools Manuf.* 1997, 37(9): 1201-1217.
[41] Liu C, Li Y, Zhou G, Shen W. A sensor fusion and support vector machine based approach for recognition of complex machining conditions. *J Intell Manuf.* 2018, 29(8):1739-1752.
[42] Huang PM, Lee CH. Estimation of Tool Wear and Surface Roughness Development Using Deep Learning and Sensors Fusion. *Sensors* 2021, 21(16): 5338.
[43] Cheng C, Wang Z, Hung W, Bukkapatnam STS, Komanduri R. Ultra-precision Machining Process Dynamics and Surface Quality Monitoring. *Procedia Manuf.* 2015, 1:607-618.
[44] Benardos PG, Vosniakos GC. Predicting surface roughness in machining: a review. *Int. J. Mach. Tools Manuf.* 2003, 43:833-844.
[45] Hassani H. A brief introduction to singular spectrum analysis. presented at the Optimal decisions in statistics and data analysis, 2010. [Online]. Available: https://ssa.cf.ac.uk/ssa2010/a_brief_introduction_to_ssa.pdf
[46] Abellan-Nebot JV, Romero Subirón F. A review of machining monitoring systems based on artificial intelligence process models. *Int J Adv Manuf Technol* 2010, 47(1-4): 237-257.
[47] Brunton SL, Noack BR, Koumoutsakos P. Machine Learning for Fluid Mechanics. *Annu. Rev. Fluid Mech.* 2019, 52: 477-508.
[48] De Lorenzis L, Nanni A. International workshop on preservation of historical structures with FRP composites. *NSF*, Jul. 2004.
[49] Hung YY. Shearography: a new optical method for strain measurement and nondestructive evaluation. *Opt. Eng.* 1982, 21:391-395.
[50] Sharp B. Electronic speckle pattern interferometry. *Opt. Laser. Eng* 1989, 21: 241-255.
[51] Hung YY. Digital shearography *versus* TV-holography for nondestructive evaluation. *Opt. Laser. Eng* 1997, 26: 421-436.
[52] Cloud G. Optical methods in experimental mechanics. 2017, 27: 19-22.
[53] Hung M. Shearography and Applications in Nondestructive Evaluation. presented at the 16th World Conference on NDT, Montreal, Canada, Sep. 2004.
[54] Xiaoran C, Meybodi K. Structural Health Monitoring by Laser Shearography. presented at the Conference Proceedings of the Society for Experimental Mechanics Series, in 6. 2015, pp. 149-156.
[55] Haridas A, Song C, Chan K, Murukeshan VM. Nondestructive characterization of thermal damages and its interactions in carbon fibre composite panels. *Fatigue Fract Eng Mater Struct* 2017, 40: 1562-1580.
[56] Sirohi RS. Optical Methods of Measurement: Wholefield Techniques. Second. CRC press, 2017.
[57] Hung YY. Shearography for non-destructive evaluation of composite structures. *Opt. Laser. Eng* 1996, 24: 161-182.
[58] Zhang Y. The importance of borescope detection work in the engine maintenance. *Aviat. Maint. Eng.* 2004, 1: 24-25.
[59] Samsonov P. Remote visual inspection for NDE in power plants. *Mater. Eval* 1993, 51:662-663.
[60] Hirose S, Ikuta K, Tsukamoto M. Development of a shape memory alloy actuator (Measurement of material characteristics and development of active endoscopes). *Adv. Robot.* 1990, 4: 3-27.
[61] Kaplan H. A borescope that behaves like the human eye. *Photon Spectra* 1994, 28:46-47.

[62] Wu S, Zhao JH, Huang ZJ. The application of measureable video endoscope in non-destructive testing. . 2000, 3, 57-60 (in Chinese). *Aerosp. Mater. Technol* 2000, 3: 57-60.
[63] Ross I. Anglo Japanese Collaboration in the Design of Medical and Industrial Endoscopic Equipment. in *In Proceedings of The Industrial Benefits of Mechatronics*, Savoy place, London, UK, Oct. 1998, p. 5/1-5/2.
[64] Yu H. Borescope and its application in aero engine maintenance. *Aeronaut. Manuf. Technol* 2005, 99:94-96.
[65] Schurr MO, Kunert W, Arezzo A. The role and future of endoscopic imaging systems. *Endoscopy* 1999, 31:557-562.
[66] Zhu YK, Tian GY, Lu RS, Zhang H. A Review of Optical NDT Technologies. *Sensors* 2011, 11: 7773-7798.
[67] Sfarra S, Ibarra-Castanedo C, Avdelidis NP. A comparative investigation for the non-destructive testing of honeycomb structures by holographic interferometry and infrared thermography. *J. Phys* 2010, 214.
[68] Xavier M. Infrared Methodology and Technology [M]. *In Nondestructive Testing Monographs and Tracts* 1992 vol. 7. New York, NY, USA: Gordon and Breach Science Publishers.
[69] Inagaki T, Ishii T, Iwamoto T. On the NDT and E for the diagnosis of defects using infrared thermography. *NDT E Int* 1999, 32: 247-257.
[70] Wilson J, Tian GY, Mukriz I, Almond D. PEC thermography for imaging multiple cracks from rolling contact fatigue. *NDT & E Int.* 2011, 44: 505-512.
[71] Röntgen WC. On a New Kind of Rays. *Science* 1896, 3(59): 227-231.
[72] Mahesh M. Use of full body scanners at airports. *BMJ* 2010, 340(7745): 490-491.
[73] Sprawls P. Physical Principles of Medical Imaging. Aspen Publishers, 1987. [Online]. Available: https://w3.aapm.org/pubs/documents/SprawlsPPMI2.pdf
[74] Hounsfield GN. Computerized transverse axial scanning (tomography): Part I. Description of system. *British Journal of Radiology* 1973, 46: 1016-1022.
[75] Fleischmann D, Boas FE. Computed tomography—old ideas and new technology. *Eur Radiol* 2011, 21(3): 510-517.
[76] Willemink MJ, Noël PB. The evolution of image reconstruction for CT—from filtered back projection to artificial intelligence. *Eur Radiol* 2019, 29(5): 2185-2195.
[77] Withers PJ, *et al.* X-ray computed tomography. *Nat Rev Methods Primers* 2021, 1(1): 18.
[78] Kak AC, Slaney M. Principles of computerized tomographic imaging. *Sociery for Industrial and Applied Mathematics* 2001.
[79] Thompson A, Maskery I, Leach RK. X-ray computed tomography for additive manufacturing: a review. *Meas. Sci. Technol.* 2016, 27(7): 072001.
[80] Pyka G, Kerckhofs G, Braem A, Mattheys T, Schrooten J, *et al.* Novel micro-ct based characterization tool for surface roughness measurements of porous structures. presented at the SkyScan User Meeting 2010, 2010.
[81] Triantaphyllou A, *et al.* Surface texture measurement for additive manufacturing. *Surf. Topogr.: Metrol. Prop.* 2015, 3(2): 024002.
[82] Kerckhofs G, Pyka G, Moesen M, Van Bael S, Schrooten J, *et al.* High-Resolution Microfocus X-Ray Computed Tomography for 3D Surface Roughness Measurements of Additive Manufactured Porous Materials. *Adv. Eng. Mater.* 2013, 15(3): 153-158.
[83] Townsend A, Pagani L, Scott P, Blunt L. Areal surface texture data extraction from X-ray computed tomography reconstructions of metal additively manufactured parts. *Precis. Eng.* 2017, 48: 254-264.

[84] Zanini F, Pagani L, Savio E, Carmignato S. Characterisation of additively manufactured metal surfaces by means of X-ray computed tomography and generalised surface texture parameters. *CIRP Annals* 2019, 68(1): 515-518.
[85] Thompson A, Körner L, Senin N, Lawes S, Maskery I, *et al.* Measurement of internal surfaces of additively manufactured parts by X-ray computed tomography. presented at the 7th Conference on Industrial Computed Tomography, Leauven, Belgium, 2017.
[86] Kantzos CA, Cunningham RW, Tari V, Rollett AD. Characterization of metal additive manufacturing surfaces using synchrotron X-ray CT and micromechanical modeling. *Comput Mech* 2018, 61(5): 575-580.
[87] Klingaa CG, Dahmen T, Baier S, Mohanty S, Hattel JH. X-ray CT and image analysis methodology for local roughness characterization in cooling channels made by metal additive manufacturing. *Addit. Manuf.* 2020, 32: 101032.
[88] Klingaa CG, Zanini F, Mohanty S, Carmignato S, Hattel JH. Characterization of Geometry and Surface Texture of AlSi10Mg Laser Powder Bed Fusion Channels Using X-ray Computed Tomography. *Applied Sciences* 2021, 11(9): 4304.
[89] Klingaa CG, Bjerre MK, Baier S, De Chiffre L, Mohanty S, *et al.* Roughness Investigation of SLM Manufactured Conformal Cooling Channels Using X-ray Computed Tomography. *eJNDT*, Mar. 2019.
[90] Fox JC, Kim F, Reese Z, Evans C. Complementary Use Of Optical Metrology And X-Ray Computed Tomography For Surface Finish And Defect Detection In Laser Powder Bed Fusion Additive Manufacturing. 2018.
[91] Evsevleev S, *et al.* X-ray Computed Tomography Procedures to Quantitatively Characterize the Morphological Features of Triply Periodic Minimal Surface Structures. *Materials* 2021, 14(11): 3002.
[92] Zanini F, Sbettega E, Sorgato M, Carmignato S. New Approach for Verifying the Accuracy of X-ray Computed Tomography Measurements of Surface Topographies in Additively Manufactured Metal Parts. *J Nondestruct Eval* 2019, 38(1): 12.
[93] Lifton JJ, Muhammad AA, Tan ZJ, Malcolm A. Internal Surface Roughness Measurement of Metal AM Channels via X-ray Computed Tomography: A Case Study. in *Special Issue of e-Journal of Nondestructive Testing (eJNDT)*, Dec. 2022.
[94] Lifton JJ, Liu Y, Tan ZJ, Mutiargo B, Goh XQ, *et al.* Internal surface roughness measurement of metal additively manufactured samples via x-ray CT: the influence of surrounding material thickness. *Surf. Topogr.: Metrol. Prop.* 2021, 9(3): 035008.
[95] Wang G, Yu H, De Man B. An outlook on x-ray CT research and development. *Med. Phys.* 2008, 35(3): 1051-1064.
[96] Liu YC, Ling C, Malcolm AA, Dong Z. Accuracy of replication for non-destructive surface finish measurement. *e-Journal of Nondestructive Testing* 2012, 17(03).
[97] George AF. A comparative study of surface replicas. *Wear* 1979, 57(1): 51-61.
[98] Wagner M, Issacson A, Michaud M, Bell M. A Comparison of Surface Roughness Measurement Methods for Gear Tooth Working Surfaces. *AGMA*, Oct. 2019, Accessed: Jun. 15, 2023. [Online]. Available: https://www.remchem.de/wp-content/uploads/2019/10/A-Comparison-of-Surface-Roughness-Measurement-Methods-for-Gear-Tooth-Working-Surfaces-AGMA19FTM21.pdf
[99] Baruffi F, Parenti P, Cacciatore F, Annoni M, Tosello G. Hello Hi On the Application of Replica Molding Technology for the Indirect Measurement of Surface and Geometry of Micromilled Components, Micromachines | Free Full-Text |", Accessed: Jun. 15, 2023. [Online]. Available: https://www.mdpi.com/2072-666X/8/6/195
[100] James PJ, Thum WY. The replication of metal surfaces by filled epoxy resins. *Precis. Eng.* 1982, 4(4): 201-204.
[101] Nilsson L, Ohlsson R. Accuracy of replica materials when measuring engineering surfaces. *Int. J. Mach. Tools Manuf.* 2001, 41(13): 2139-2145.

[102] Baruffi F, Parenti P, Cacciatore F, Annoni M, Tosello G. On the Application of Replica Molding Technology for the Indirect Measurement of Surface and Geometry of Micromilled Components. *Micromachines* 2017, 8(6).
[103] Macdonald DA, Harman R, Evans AA. Replicating surface texture: Preliminary testing of molding compound accuracy for surface measurements. *J. Archaeol. Sci. Rep.* 2018,18: 839-846.
[104] Liu Y, Ling CY, Malcolm A, Dong Z. Accuracy of replication for non-destructive surface finish measurement. Jan. 2011.
[105] Replica Tape Reader - PosiTector RTR | DeFelsko. https://www.defelsko.com/positector-rtr (accessed Jun. 15, 2023).
[106] Stachnik R. Replica Tape: Linearization of Roughness Measurments. Oct. 30, 2013. Accessed: Jun. 15, 2023. [Online]. Available: https://dl.defelsko.com/Testex/Linearization-RoughnessMeasurements.pdf?_gl=1*1hs2d2z*_gcl_au*MjIzNDkwNzcxLjE2ODY3MzM5NTg.*_ga*MTk1MzM4NTE3My4xNjg2NzMzOTU4*_ga_TZ8D9MBV5V*MTY4Njc0ODI4Ny4zLjAuMTY4Njc0ODI4Ny42MC4wLjA.
[107] Schmidt P. How reliable is the visual identification of heat treatment on silcrete? A quantitative verification with a new method. *Archaeol Anthropol Sci* 2019, 11(2): 713-726.